

1 **A New Stefan Equation Reveals to Characterize the Evolution of**
2 **Thermokarst Lake and Talik Geometry**~~Three-Dimensional Stefan~~
3 ~~Equation for Thermokarst Lake and Talik Geometry Characterization~~

4 **Noriaki Ohara¹, Benjamin M. Jones², Andrew D. Parsekian^{3,1}, Kenneth M. Hinkel⁴, Katsu**
5 **Yamatani⁵, Mikhail Kanevskiy², Rodrigo C. Rangel³, Amy L. Breen⁶, and Helena**
6 **Bergstedt^{2,7}**

7
8 ¹Department of Civil and Architectural Engineering, University of Wyoming, Laramie, WY,
9 82071, USA

10 ²Institute of Northern Engineering, University of Alaska Fairbanks, Fairbanks, Alaska, 99775,
11 USA

12 ³Department of Geology and Geophysics, University of Wyoming, Laramie, WY 82071, USA

13 ⁴Department of Geological and Mining Engineering and Sciences, Michigan Technological
14 University, Houghton, MI 49931, USA

15 ⁵Department of Urban Science, Meijo University, 4-102-9 Yataminami, Higashi, Nagoya 461-
16 8534, Japan

17 ⁶International Arctic Research Center, University of Alaska Fairbanks, Fairbanks, Alaska

18 ⁷[b.geos, Vienna, Austria](https://www.b.geos.ac.at/)

19 Corresponding author: Noriaki Ohara (nohara1@uwyo.edu)

20

21 Abstract

22 Thermokarst lake dynamics, which plays an essential role in carbon release due to permafrost
23 thaw, ~~are~~ affected by various geomorphological processes. In this study, we derive a three-
24 dimensional (3D) Stefan equation to characterize talik geometry under a hypothetical
25 thermokarst lake in the continuous permafrost region. Using the Euler equation in the calculus
26 of variations, the lower bounds of the talik were determined as an extremum of the functional
27 describing the phase boundary area with a fixed total talik volume. We demonstrate that the
28 semi-ellipsoid geometry of the talik is optimal for minimizing the total permafrost thaw under
29 the lake for a given annual heat supply. The model predicting ellipsoidal talik geometry was
30 verified by talik thickness observations using transient electromagnetic (TEM) soundings in
31 Peatball Lake on the Arctic Coastal Plain (ACP) of northern Alaska. The ~~lake~~-width-depth ratio
32 of the elliptical sub-lake talik can characterize the energy flux anisotropy in the permafrost,
33 although the lake bathymetry cross section may not be elliptic due to the presence of near-
34 surface ice-rich permafrost. This theory suggests that talik development deepens lakes and
35 results in more uniform horizontal lake expansion around the perimeter of the ~~stabilizes slows~~
36 horizontal expansion rates of thermokarst lakes ~~ss by ground subsidence due to permafrost thaw~~
37 while wind-induced waves and currents are likely responsible for the elongation and orientation
38 of shallow thermokarst lakes without taliks in certain regions such as the ACP of northern
39 Alaska.

40 1. Introduction

41 Thermokarst lakes are abundant in regions underlain by ice-rich permafrost including the Arctic
42 Coastal Plain (ACP) of northern Alaska, northwestern Canada, and Siberia (Grosse et al., 2013;
43 [Jones et al., 2022](#)). These lakes are formed due to permafrost degradation, and their basin
44 evolution is fundamentally different from lakes formed in temperate and tropical regions.

45 Thermokarst lakes affect the thermal regime of the surrounding permafrost, which [affects](#)
46 [controls](#) the geomorphology and evolution of the lake basin ([Brewer, 1958](#)). If the lake bed has a
47 mean annual temperature greater than 0 °C, the sub-lake permafrost will begin to thaw (Burn,
48 2002; Arp et al., 2016). This typically occurs in lakes [that are](#) deeper than the maximum winter
49 ice thickness, where the ice cover floats above an unfrozen water [body-layer](#) ([Jeffries et al.,](#)
50 [1996; Burn, 2002](#)). In this case, unfrozen lake bed sediments persist, and the thaw front
51 continues to penetrate deeper into the underlying permafrost. This [creates results in a](#) “talik”, or
52 a perpetually unfrozen zone confined by permafrost, beneath the lake depending on local
53 anomalies in thermal, hydrological, hydrogeological, or hydrochemical conditions (van
54 Everdingen, 1998). In ice-rich permafrost, the conversion of ice to water with thaw causes a
55 volumetric reduction in the unconsolidated material, and the lake bed consequently subsides
56 [significantly increasing the depth of initial basins](#) ([Czudek and Demek, 1970; Jorgenson and](#)
57 [Shur, 2007; Shur and Osterkamp, 2007; Jorgenson, 2013; French, 2018; Kanevskiy and Bjella,](#)
58 [2020](#)). The total depth of [thaw](#) subsidence is determined by the [depth-amount](#) and distribution of
59 excess-ice content in the permafrost [with depth](#). As the lake expands by lateral thermo-
60 mechanical erosion (~~thermal abrasion~~) of the banks, mineral and organic sediments from
61 retreating shores are delivered to the lake basin (Farquharson et al., 2016). However, thaw-
62 induced ground subsidence effectively deepens the basin, so volumetric capacity can [actually](#)

63 increase over time. Over decades and centuries, the talik increases in thickness, and lake bed
64 subsidence continues as long as the thawing permafrost is ice-rich ([West and Plug, 2008](#)).

65 In certain ice-rich permafrost regions in the Arctic, there is a preferential orientation and elliptic
66 shape to the ~~numerous~~ thermokarst lakes ~~that occur there~~ (Black and Barksdale, 1949; Hinkel et
67 al., 2005; Grosse et al., 2013). In particular, elliptical oriented lake districts are found
68 predominantly along the central north Siberian coast, northern Alaska and in northwest Canada
69 (Grosse et al., 2013). On the ACP of northern Alaska, many elliptical thermokarst lakes have a
70 long axeslong axis oriented 10–20 degrees west from true north, which is nearly perpendicular to
71 the prevailing wind direction ([Carson, 1968](#); Sellmann, 1975; Carter, 1981). Hinkel et al. (2005,
72 2012) also showed significant correlation between lake orientation and summer wind direction
73 by analyzing the geometric shape metrics of the thermokarst lakes and drained thermokarst lake
74 basins (DTLB) on the ACP of Alaska. It has been proposed that winds at the lake surface cause
75 currents and water waves, and generate a two-cell circulation pattern which triggers
76 thermomechanical bank erosion, resulting in asymmetrical elliptical orientation (Livingstone,
77 1954; Rex, 1961; Carson and Hussey, 1962; Mackay, 1992; Arp et al., 2011). The sublittoral
78 shelves and bars typically found in the deeper thermokarst lakes may also be formed by wind-
79 driven currents and waves, and warmer water temperatures (Carson and Hussey, 1962). The axis-
80 oriented sublittoral shelves make the orientation appear more pronounced in larger basins. Other
81 processes also influence the orientation of thermokarst lakes such as historical drained lake
82 geometry, ground ice distribution, and dune ridge orientation by aeolian sand transport (Carter,
83 1981).

84 Several numerical models have been proposed and applied that describe permafrost thaw for the
85 purpose of analyzing water and carbon cycles (e.g., Kessler et al., 2012). However, Schuur et al.

86 (2015) stress the need to better represent talik formation and geometries to ~~more effectively~~
87 parameterize numerical models more effectively. Painter et al. (2016) demonstrated a coupled
88 surface/subsurface permafrost thermal hydrology model at the multiple ice-wedge polygon scale.
89 Kessler et al. (2012) simulated carbon mobilization over 10,000 years on two neighboring thaw
90 lakes located on ice- and organic-rich Yedoma permafrost terrains (Kanevskiy et al., 2011;
91 Schirrmeister et al., 2013) in the northern Seward Peninsula, Alaska using a 3D numerical
92 thermal model. They demonstrated the effectiveness of model simulations for methane emission
93 from thermokarst lakes. Ling and Zhang (2003b) provided a numerical parametrization of lake
94 talik development, and showed that shallow thermokarst lakes are a significant heat source
95 affecting permafrost and talik geometries. Rowland et al. (2011) advanced the technique by
96 including ~~parameter of~~ advective heat transport on talik evolution. West and Plug (2008) and
97 Plug and West (2009) characterized the lake bathymetry including the effects of lake ice and
98 littoral shelves. These thermal models use long-term mean lake temperature as the Dirichlet
99 boundary condition and a uniform annual mean temperature profile as the initial condition.
100 Analytical and numerical models can provide dynamic solutions for the heat transfer equation
101 under quasi-steady state climate conditions. However, the existing models require prescribed
102 lake shapes (circle or ellipse) to obtain information on talik depths as opposed to modeling the
103 likely influence of talik evolution on lake shape – this work, in part, attempts to address this
104 shortcoming.

105 Direct drilling measurements of taliks below thermokarst lakes are difficult to obtain and only
106 exist in a few rare case studies (Brewer, 1958; Johnston and Brown, 1966; Roy-Leveilee and
107 Burn, 2017; Heslop et al., 2015). Geophysical methods can be used (e.g., Schwamborn et al.,
108 2000; Parsekian et al., 2019; Creighton et al., 2018; Sullivan et al., 2021; O’Neill et al., 2020);

109 however, it is time consuming and laborious to produce 3D subsurface images at the large scale
110 of lakes found in permafrost lowland regions. Since field measurements (coring, geophysics,
111 etc.) are spatiotemporally limited, numerical and analytical modelling is used to gain critical
112 insights into talik evolution. Mackay (1962) obtained the analytical vertical temperature profiles
113 below the water at the center of a circular lake by analytically solving the heat transfer equation.
114 Burn (2002) subsequently extended the solution for an elongated lake. This analytical model has
115 been used for lake process characterization because the quasi-steady state model was able to
116 reasonably quantify the talik thickness. For example, Hinkel and Arp (2015) applied the
117 temperature profile to 2100 lakes and found that larger, long-lived lakes (more than 66 ha) may
118 have taliks that penetrate through the permafrost ([throughgoing-open taliks](#)) to the ground-water
119 system below in a region with permafrost that is up to 600 m thick.

120 These existing models require the prescribed lake shapes (circle or ellipse) to obtain the talik
121 depth; in fact, no existing studies explicitly provide an answer to the fundamental question: why
122 do thermokarst lakes tend to be elliptical and/or round? Also, in spite of several decades of
123 research focused on the orientation of thermokarst lakes in certain regions, no existing studies
124 explicitly explain why thermokarst lakes in some regions orient perpendicular to the prevailing
125 wind direction. The objective of this work is to implement a novel mathematical framework that
126 concurrently describes both the oriented nature of the thermokarst lakes and the talik depth
127 below the lakes. Previous models have calculated the talik development due to heat flow, though
128 most use some simplifying assumptions to reduce dimensionality. Separately, researchers have
129 hypothesized about elliptical lake morphology by invoking winds, currents, and erosion. Here,
130 we couple both the talik evolution and lake shape questions together in a single mathematical
131 model. Additionally, we intend to use this theory to demonstrate that the thermal gradient could

132 exert control on the depth/width ratio of the talik. In other words, the proposed theory aims to
133 isolate the most important process – sub-lake permafrost thaw and subsidence – from other
134 effects such as wind-wave erosion, thaw slumping, sediment redistribution and incoming
135 radiation imbalance, using thermally optimized lake geometry.

136 **2. Theory**

137 **2.1 Basin integrated energy equation**

138 The approach used in this study is based on the Lagrangian mechanics, which generalizes the
139 classical Newtonian mechanics, using the stationary action principle (the principle of least
140 action). The action is defined as the integral of the Lagrangian, which consists of kinetic and
141 potential energy of the system. In this application, the Lagrangian simply becomes the potential
142 energy due to absence of kinetic energy. The variational principle that is the main tool in
143 Lagrangian mechanics can indeed derive the equations in the Newtonian mechanics. One of the
144 related research topics using the variational principle to fluid mechanics is a phase boundary
145 propagation, which can be analyzed by the phase field model or diffusion-interface model
146 (Cassel, 2013). This model explains the diffuse phase boundary without surface tension that
147 appeared in Newtonian interfacial physics between a liquid and a gas. According to the second
148 law of thermodynamics, the free energy of the system must decrease monotonically to ensure a
149 non-negative entropy production (Singer-Loginova and Singer, 2008). This needsrequiresrequires
150 that the time rate of change of the phase boundary be expressed by the functional derivative of
151 the free energy functional, which corresponds to the talik total energy flux in relation to
152 permafrost thaw problem. This study directly and analytically solves the Euler-Lagrange

153 equation based on the stationary action principle rather than the entropy functional used in the
 154 phase field method.

155 Heat energy collected by a waterbody is used for phase boundary expansion as well as heat
 156 conduction into the adjacent permafrost (e.g., French, 19962018). From the energy balance
 157 equation around the phase boundary, the energy for permafrost thaw is expressed as the
 158 subtraction of heat conduction from the input energy at the phase boundary (Carslaw and Jaeger,
 159 1959; Patel, 1968; Lunardini, 1981). The material of permafrost and talik is assumed to be fully
 160 saturated with ice and water, respectively. Also, the thermal constants (thermal conductivity,
 161 latent heat, and thawing temperature) are constant and isotropic, and the change in volume of
 162 water on thawing and freezing is negligible. ThereforeUnder such assumptions, the energy
 163 conservation equation at the phase boundary can be expressed as,

$$164 \quad \phi v \rho L q_f = q_{suf} - k_L \frac{dT}{dn} q_{in} - \left(-k_p \frac{dT}{dn} \right) q_e, \quad \text{--- (1)}$$

165 where ϕ is volumetric water content (m^3/m^3); v is thaw rate or advancement of talik boundary
 166 (m/s); ρ is density of water (kg/m^3); L is latent heat for ice thaw (liquid-solid) (J kg^{-1}); q_{suf} is
 167 additional heat input from ground surface around the lake shore (W/m^2); k_L is thermal
 168 conductivity of unfrozen soil ($\text{W}/(\text{m}\cdot\text{C})$); and k_p is thermal conductivity of frozen soil
 169 (permafrost) ($\text{W}/(\text{m}\cdot\text{C})$); T is temperature (C); and n is outward normal from the interface into
 170 the soil (m). The energy terms can be grouped into where q_f is heat for permafrost fusion or
 171 thawing q_{th} (W/m^2); q_{in} is incoming heat input at the phase boundary q_{in} (W/m^2); and q_e is
 172 outgoing heat by conduction to the permafrost q_{out} (W/m^2). These heat fluxes can be evaluated
 173 by the following formulas:

174
$$q_{thf} = \phi v \rho L \quad , \quad (2)$$

175
$$q_{in} = q_{surf} - k_L \frac{dT}{dn} \quad , \text{ and} \quad (3)$$

176
$$q_{oute} = -k_p \frac{dT}{dn} \quad . \quad (4)$$

177 where ϕ is volumetric water content; v is thaw rate or advancement of talik boundary (m/s); ρ is
 178 density of water (kg/m^3); L is latent heat for fusion (liquid-solid) of water (J kg^{-1}); q_{surf} is
 179 additional heat input from ground surface around the lake shore (W/m^2); k_L is thermal
 180 conductivity of unfrozen soil or lake water; and k_p is thermal conductivity of frozen soil
 181 (permafrost); T is temperature ($^{\circ}\text{C}$); and n is outward normal from the interface into the soil (m).

182 When heat input from the surface is consumed for phase change without any loss ($q_{oute} =$
 183 $q_{surf} = 0$), the well-known Stefan equation can be obtained from Equations (1) through (4) under
 184 the quasi-steady state approximation (Stefan, 1891; Kurylyk & Hayashi, 2016). This study also
 185 adopts the quasi-steady state approximation for the talik shape characterization.

186 As the thawing process is direction-dependent, it is convenient to use vector notation (Figure 1).
 187 That is,

188
$$\mathbf{q}_{thf} = \mathbf{q}_{in} - \mathbf{q}_{oute} \quad . \quad (5)$$

189 A vector is denoted by the letter **a** in bold letter denotes a vector. The fusion-talik expansion heat
 190 flux vector corresponds to thaw direction, which is affected by the other two heat fluxes. Figure
 191 1 ~~also~~ illustrates the thermal profiles around the thaw lake in warm and cold seasons. The
 192 horizontal near-surface heat conduction is influenced by the seasonality of the surface heat
 193 budget while the vertical heat conduction under the lake remains unidirectional throughout the
 194 years. Clearly, the presence of the thaw lake considerably alters the heat environment of the

195 permafrost while the temperature slope at the bottom of the permafrost may be approximated by
 196 the geothermal gradient in regions with thick continuous permafrost such as the ACP.- This
 197 directionality in the heat environment around the lake may cause anisotropic talik expansion.
 198 Here, the phase change heat vector is expressed as proportional to the normal heat input q_{in} , as
 199 follows:

$$200 \quad \mathbf{q}_{thf} = (q_{thf,x}, q_{thf,y}, q_{thf,z}) = (\xi q_{in}, \eta q_{in}, \zeta q_{in}) = q_{in}(\xi, \eta, \zeta) \text{-----} \quad (6)$$

201 where q_{in} is the input heat normal to the phase boundary, ξ , η , and ζ are the ~~fusion-thaw~~ energy
 202 fractions of the heat input normal to the phase boundary with respect to x, y, and z directions,
 203 respectively. The depth of the phase boundary (m), $z = \varphi(x, y)$, may be expressed as an
 204 arbitrary 3D surface as,

$$205 \quad g(x, y, z) = \varphi(x, y) - z = 0. \quad (7)$$

206 Hence, the normal vector \mathbf{n} at any location on the phase boundary g can be written as follows:

$$207 \quad \mathbf{n} = \frac{\nabla g}{|\nabla g|} = \frac{1}{|\nabla g|} (g_x, g_y, g_z) = \frac{1}{\sqrt{\varphi_x^2 + \varphi_y^2 + 1}} (\varphi_x, \varphi_y, -1) \quad (8)$$

208 where the subscript in this expression denotes partial derivative (e.g. $\varphi_x = \partial\varphi/\partial x$) and ∇ is a
 209 vector differential operator ($\partial/\partial x, \partial/\partial y, \partial/\partial z$). As such, the vector of the input heat to the
 210 phase boundary φ is

$$211 \quad \mathbf{q}_{in} = |\mathbf{q}_{in}| \mathbf{n} = q_{in} \mathbf{n} = \frac{q_{in}}{\sqrt{\varphi_x^2 + \varphi_y^2 + 1}} (\varphi_x, \varphi_y, -1), \quad (9)$$

212 and the corresponding ~~fusion-thaw~~ heat vector is,

213
$$\mathbf{q}_{thf} = \frac{q_{in}}{\sqrt{\varphi_x^2 + \varphi_y^2 + 1}} (\xi \varphi_x, \eta \varphi_y, -\zeta). \quad (10)$$

214 Next, the fusion-thaw heat magnitude can be evaluated using a Euclidian norm as,

215
$$|\mathbf{q}_{thf}| = \frac{q_{in}}{\sqrt{\varphi_x^2 + \varphi_y^2 + 1}} \sqrt{\xi^2 \varphi_x^2 + \eta^2 \varphi_y^2 + \zeta^2} = \frac{\zeta q_{in}}{\sqrt{\varphi_x^2 + \varphi_y^2 + 1}} \sqrt{\alpha_x^2 \varphi_x^2 + \alpha_y^2 \varphi_y^2 + 1} \quad (11)$$

216 where

217
$$\alpha_x = \frac{\xi}{\zeta}, \quad \alpha_y = \frac{\eta}{\zeta} \quad . \quad (12)$$

218 The α -parameters α_x and α_y (unitless ratio) describe the anisotropic thermal condition between
 219 horizontal and vertical directions. The parameters α_x and α_y are greater than one when the
 220 vertical temperature gradient is steeper than in horizontal directiongradient. The total fusion
 221 thaw energy over the lake can be computed by the area integral on the phase boundary Γ . That
 222 is,

223
$$\int_{\Gamma} |\mathbf{q}_{thf}| d\Gamma = \iint_B |\mathbf{q}_{thf}| \sqrt{\varphi_x^2 + \varphi_y^2 + 1} dx dy$$

 224
$$= \zeta q_{in} \iint_B \sqrt{\alpha_x^2 \varphi_x^2 + \alpha_y^2 \varphi_y^2 + 1} dx dy. \quad (13)$$

225 This expression indicates that the heat required for lake expansion is proportional to the weighted
 226 phase boundary area with the weights α_x and α_y .

227 **2.2 Optimum phase boundary shape-shapeas-extremum**

228 The calculus of variation, often referred to as a functional analysis, is the mathematical technique
 229 to find an extremum (minimum or maximum) of the system in terms of a function type instead of
 230 a variable (e.g., Courant and Hilbert, 1954; Gelfand and Fomin, 1963). There, we present the

231 thermally optimum function types $\varphi(x, y)$ of the phase boundary can be derived using this
 232 method. As presented in the previous section, the heat consumption rate for talik expansion is
 233 represented by the weighted phase boundary area while the time-integrated heat supply is
 234 equivalent to the thawed permafrost volume. Assuming heat thaws the most susceptible region
 235 of the permafrost near the heat source first, the shape of a talik may minimize the total
 236 permafrost thaw with a given amount of incoming energy. ~~Hence~~In other words, as the free
 237 energy of the system must decrease monotonically to ensure a non-negative entropy production
 238 (the second law of thermodynamics),~~this variational principle states that~~ the optimum talik
 239 shape should minimize the phase boundary area for a specified talik volume ~~the total talik~~
 240 ~~expansion~~. The weighted phase boundary area A and its volume V can be expressed as follows:

$$241 \quad \begin{cases} V[\varphi] = \iint_B \varphi \, dx dy \\ A[\varphi] = \iint_B \sqrt{\alpha_x^2 \varphi_x^2 + \alpha_y^2 \varphi_y^2 + 1} \, dx dy \end{cases} \quad (14)$$

242 To obtain the optimum talik shape, ~~t~~The functional F is formulated using the method of
 243 Lagrange multipliers ~~defined as,~~

$$244 \quad F[\varphi] = \lambda V[\varphi] + A[\varphi] = \iint_B (\lambda \varphi + \sqrt{\alpha_x^2 \varphi_x^2 + \alpha_y^2 \varphi_y^2 + 1}) \, dx dy \quad (15)$$

245 where λ is a the Lagrange multiplier ~~constant~~. The Extremum ~~m~~Minimum of the functional F
 246 can be determined for $\lambda < 0$ because both V and A are monotonic functions. Let

$$247 \quad f(\varphi, \varphi_x, \varphi_y) = \lambda \varphi + \sqrt{\alpha_x^2 \varphi_x^2 + \alpha_y^2 \varphi_y^2 + 1}. \quad (16)$$

248 Equation (15) becomes,

$$249 \quad F[\varphi] = \lambda V[\varphi] + A[\varphi] = \iint_B f(\varphi, \varphi_x, \varphi_y) \, dx dy. \quad (17)$$

250 Note that this functional can be interpreted as the Lagrangian of the system. Therefore, to find
 251 the extremal phase-boundary shape φ that minimizes the functional $F[\varphi]$, the Euler-Lagrange
 252 equation Euler's Equation can be formulated as,

$$253 \quad \frac{\partial f(\varphi, \varphi_x, \varphi_y)}{\partial \varphi} - \frac{\partial}{\partial x} \left(\frac{\partial f(\varphi, \varphi_x, \varphi_y)}{\partial \varphi_x} \right) - \frac{\partial}{\partial y} \left(\frac{\partial f(\varphi, \varphi_x, \varphi_y)}{\partial \varphi_y} \right) = 0. \quad (18)$$

254 Substituting Equation (16) to (18) yields,

$$255 \quad \lambda - \frac{\partial}{\partial x} \left(\frac{\alpha_x^2 \varphi_x}{\sqrt{1 + \alpha_x^2 \varphi_x^2 + \alpha_y^2 \varphi_y^2}} \right) - \frac{\partial}{\partial y} \left(\frac{\alpha_y^2 \varphi_y}{\sqrt{1 + \alpha_x^2 \varphi_x^2 + \alpha_y^2 \varphi_y^2}} \right) = 0. \quad (19)$$

256 By analogy to two-dimensional application in Ohara and Yamatani (2019), an ellipsoid is one of
 257 the solutions of Equation (19), as follows:

$$258 \quad z = -\varphi = -\sqrt{\frac{4}{\lambda^2} - \frac{x^2}{\alpha_x^2} - \frac{y^2}{\alpha_y^2}} + d, \text{ or} \quad (20)$$

$$259 \quad \left(\frac{x}{\frac{2\alpha_x}{|\lambda|}} \right)^2 + \left(\frac{y}{\frac{2\alpha_y}{|\lambda|}} \right)^2 + \left(\frac{z-d}{\frac{2}{|\lambda|}} \right)^2 = 1. \quad (21)$$

260 Detailed alternative derivation using isoperimetric inequality is available in the Appendix A. The

261 coefficients d and λ can be determined by further variational analysis explained in Appendix B.

262 As such, Equations (20) and (21) become

$$263 \quad \varphi = \sqrt{D^2 - \frac{x^2}{\alpha_x^2} - \frac{y^2}{\alpha_y^2}}, \text{ and} \quad (22)$$

$$264 \quad \left(\frac{x}{\alpha_x D} \right)^2 + \left(\frac{y}{\alpha_y D} \right)^2 + \left(\frac{z}{D} \right)^2 = 1, \text{ respectively.} \quad (23)$$

265 D is the talik center depth, α_x & α_y are the cross-sectional aspect ratios. Hence, the semi-
 266 ellipsoidal geometry of the phase boundary (i.e., the boundary between the permafrost and talik)
 267 was explicitly derived as a thermally optimum shape based on the variational principle using the
 268 thermal quasi-steady state approximation. As the Stefan equation describes the phase boundary
 269 depth (active layer depth or frost depth) under a uniform and flat ~~flat~~ landscape, the solution of
 270 the Euler-Lagrange equation (Equation 22) ~~this~~ is the 3D Stefan Equation for the talik beneath a
 271 thermokarst lake.

272 **2.3 Thermokarst lake bathymetry and phase boundary geometry**

273 When top-down permafrost thaw dominates the process, the thermokarst lake bottom shape
 274 $\psi(x, y)$ may be similar to the phase boundary shape, as illustrated in Figure 2. However, the
 275 lake bathymetry can be related to the permafrost degradation rate r_{deg} (ratio; m/m) defined as,

$$276 \quad r_{deg} = \frac{D_{thaw}}{D_{frzn}} \sim 1 - \frac{\psi(x,y)}{\varphi(x,y)} \sim 1 - \frac{H}{D} \quad , \quad (24)$$

277 where H and D denote the water depth and the talik thickness at the lake center, respectively.

278 D_{frzn} is the frozen soil thickness (m) and D_{thaw} is the corresponding thawed soil thickness depth
 279 (m), which is strongly dependent on the excess ground ice content; excess ice is defined as the
 280 volume of ice in the ground, which exceeds the total pore volume that the ground would have
 281 under natural unfrozen conditions (van Everdingen, 1998; Kanevskiy et al., 2013). Therefore,
 282 thaw settlement is typically computed from wedge excess-ice volume content and the thickness of
 283 the layer with excess ground ice. However, as the consolidation settlement effect, which is a
 284 function of void ratio and effective stress, may not be separated, we use the simple permafrost
 285 degradation rate (Equation 24) in this study.

286 If the permafrost degradation rate is uniform and constant throughout the basin (Panel A:
 287 uniform permafrost in Figure 2), the lake bathymetry tends to be an ellipsoid shape. However, as
 288 the ice-rich layer (~~ice wedges~~) is typically developed near the surface on the ACP (e.g.,
 289 Kanevskiy et al., [2011](#), [2013](#), [2016](#)), the bathymetry may have a flatter bottom like a rectangular
 290 cross section (Panel B: layered permafrost in Figure 2) because the ice-rich layer is characterized
 291 by much higher thaw settlement than the ice-poor permafrost at depth. Therefore, proportionality
 292 between talik thickness and lake water depth ~~or uniform permafrost~~ is unlikely reasonable
 293 assumption due to the ice-rich layer presence. Indeed, Hinkel et al. (2012) showed many flat-
 294 bottomed lakes through the extensive bathymetry surveys across the ACP of Alaska using a
 295 GPS-enabled sonar from a boat.

296 Additionally, as hydrology also affects the lake water level, the apparent lake bathymetry or lake
 297 water depth, $h(x, y)$ must be adjusted by the water loss (or gain) per unit area. Therefore,

$$298 \quad h(x, y) = [1 - r_{degsub}] \varphi(x, y) - H_{loss} \quad , \quad (25)$$

299 where H_{loss} (m) is the elevation difference between the current water surface and original ground
 300 surface before lake formation. At the lake center,

$$301 \quad H = [1 - r_{degsub}] D - H_{loss} \quad . \quad (26)$$

302 Thus, the thermokarst lake bathymetry is affected by the ice-rich layer thickness, interannual
 303 water balance, lake age, and talik geometry.

304 **3. Case study**

305 **3.1 Study area**

306 Peatball Lake (70°42.40N, 153°55.50W; 3 m above sea level) on the ACP of Alaska was chosen
307 for the demonstrative model application in this study as it has been relatively well documented
308 [in previous studies \(Lenz et al. 2016; Creighton et al., 2018; Parsekian et al., 2019\)](#). Figure 3
309 shows the location of Peatball Lake [within the Teshekpuk Lake subregion](#), as well as ~~the other~~
310 subregions that will be ~~presented-discussed~~ later.

311 Peatball Lake, named for the abundant submerged peat balls on the lake bed, is a subcircular lake
312 on the Outer Coastal Plain of Alaska with a surface area of 1.18 km². Permafrost in this area is as
313 thick as ~~~40~~40 m (Jorgenson et al., ~~2007~~2008), and the average volumetric ground ice content is
314 about 77% in the near surface to a depth of 4 m (Kanevskiy et al., 2013~~4~~). A talik has formed
315 under Peatball Lake because the maximum water depth of 2.5 m exceeds the maximum winter
316 ice thickness of 1.5 to 2.0 m (Arp et al., 2015; Lenz et al., 2016). The talik depth was estimated
317 as 91 m at the lake center based on noninvasive TEM measurements (Creighton et al., 2018).
318 However, the talik may not be present beneath the [shallow](#) sublittoral shelves on the western
319 shore [determined](#) from the bathymetry (Lenz et al., 2016). Additionally, Lenz et al. (2016)
320 reported that, based on remote sensing imagery, Peatball [L](#)lake has expanded laterally between
321 0.02 ~~m/year~~ and 1.36 m/year [between-from](#) 1955 [and-to](#) 2002.

322 **3.2 Geophysical survey of talik**

323 Geophysical field methods are effective for identifying and visualizing the frozen-unfrozen
324 interface, which is a key feature in permafrost dynamics (e.g., Pilon et al., 1985; Doolittle et al.,
325 1990; O'Neill et al., 2020; Rangel et al., 2021). For [sub](#)-lake taliks in the continuous permafrost

326 zone, Schwamborn et al. (~~2002~~2000) analyzed the sedimentary history of Lake Nikolay in the
327 western Lena River Delta using seismic reflection and ground penetrating radar (GPR). Other
328 geophysical methods such as surface nuclear magnetic resonance (NMR) can be used to detect
329 lake taliks (Parsekian et al., 2019) and remnant taliks in drained lake basins (Rangel et al., 2021).
330 At Peatball Lake, Creighton et al. (2018) estimated the talik depth using transient
331 electromagnetic (TEM) surveys along transects perpendicular to lakeshores. The dataset at
332 Peatball Lake is, to our knowledge, the only quasi-3D talik depth model available under an
333 isolated lake in the continuous permafrost in the Arctic zone because others are mostly sporadic
334 talik depth measurements at single drill points.

335 We applied the derived 3D Stefan equation to Peatball Lake based on ~~the~~ 27 talik thickness point
336 measurements across the lake (Figure 4), estimated using TEM soundings (Creighton et al.,
337 2018) during spring 2016 and 2017. Figure 4 shows the observed talik thicknesses by the TEM
338 sounding (dots) and the fitted theoretical talik thickness estimates (contour lines) superimposed
339 over the corresponding lake bathymetry measured by Lenz et al. (2016).

340 The geometric parameters of the semi-ellipsoid model such as the talik center depth (D), the
341 cross-sectional aspect ratios (α_x & α_y), lake orientation azimuth angle and the lake center
342 location were systematically determined by grid searching to minimize the root mean square
343 difference (RMSD) between the model and thaw front obtained from the TEM data. The
344 optimum parameters for the smallest RMSD (5.94 m) are shown in Figure 4. Unexpectedly, the
345 basin orientation angle was found to be 23 degrees east from true north, unlike the orientation of
346 other surrounding lakes in the region. Comparison between the extrapolated talik geometry and
347 the lake bathymetry (Lenz et al., 2016) suggests the possibility of coalescence of two basins in
348 the past; a relatively common occurrence on the ACP of Alaska. However, if we had more TEM

349 measurement points, particularly in the “possible talik sub-basin”, the fitted talik geometry could
350 be different as the model was only fitted for the 27 TEM soundings. Lake taliks tend to have a
351 semi-ellipsoidal shape, at least locally, as indicated by the very good fit of the elliptic model to
352 the TEM measured talik thicknesses (see Figure 4 with overall RMSD = 5.94 m). The idealized,
353 thermally optimum ~~model~~ geometry ~~model~~ can be used to analyze lake formation history of the
354 irregular talik associated with multi-generation lakes such as Peatball Lake.

355 Additionally, the gaps between the shoreline and the modeled talik extent located along north
356 and east shores occur where lake expansion is ~~occurring~~ most rapidly (Lenz et al., 2016). It has
357 been reported that thaw lake banks continuously retreat through a combination of thermal and
358 mechanical processes, although there is significant variability in rate of bank retreat depending
359 on region (Hopkins, 1949; Hopkins et al., 1955; Tomirdiaro, 1982; Rampton, 1982; Burn and
360 Smith, 1990; Jones et al. 2011, Lenz et al., 2016). Cross-sectional numerical thermal models
361 demonstrated that the expansion rates are affected by the talik thickness (Plug and West, 2009)
362 and seasonal snow cover (Ling and Zhang, 2003a). The disagreement between the lake and talik
363 extents on the north and east shores of Peatball ~~L~~lake implies that rapid horizontal lake
364 expansion can locally dominate permafrost thaw and subsidence processes even in a lake with a
365 talik.

366 Figure 5 compares the observed lakebed and talik profiles in Peatball Lake along the north-south
367 center line and along transects (b) – (c), respectively. Note that the TEM transects for the talik is
368 not a straight line (See ~~figure~~ Figure 4); therefore, the fitted theoretical line shows irregularity.
369 Figure 5A illustrates that the lakebed profile is characterized by flatter trapezoidal geometry
370 compared to the elliptic talik. In fact, there is a clear inflection in the linear regression line at a
371 talik depth of ~50 m in Figure 5B. From the slopes of the regression lines, the permafrost

372 degradation rates r_{deg} are computed as 97.3 % and 99.7 % for the shallow talik section (50 m or
 373 less) and the deep section (50 m or more), respectively. This analysis suggests that the
 374 subsidence due to permafrost thaw continues even after the shallow ice-rich part of the
 375 permafrost (about 4 meters, Kanevskiy, 2013~~4~~) is thawed while it has diminished around the
 376 depth of 50 meter under Peatball Lake. This case study demonstrates a link between lake
 377 bathymetry and talik thickness associated with a layered permafrost structure ~~and the wind~~
 378 ~~erosion effect~~.

379 3.3 Depth-width ratio and temperature gradient

380 The analysis (Equations 22 & 23) suggests the proportional relationship between lake/talik
 381 geometry and thaw energy. That is,

$$382 \quad a : b : D = \alpha_x : \alpha_y : 1 = \xi : \eta : \zeta = q_{f,x} : q_{f,y} : q_{f,z} \quad . \quad (27)$$

383 Combining Equations (27), (1) and (4), the depth-width (radius) ratio of the talik may be written
 384 as follows:

$$385 \quad a : D = \left(q_{in,x} + k_p \frac{dT}{dr} \right) : \left(q_{in,z} + k_p \frac{dT}{dn} \right) \quad (28)$$

386 where r and n are the horizontal and vertical distances from the original permafrost surface
 387 center, respectively, and a is the representative horizontal radius of the lake. This expression
 388 states that the anisotropic top-down permafrost thaw is caused by anisotropy of the thermal
 389 gradient for uniform incoming energy and uniform thermal properties of near surface
 390 permafrost. For example, since the vertical thermal gradient is typically steeper than the
 391 horizontal gradient during the critical summer months (Carson and Hussey, 1962; illustration in
 392 Figure 1), the heat energy in the vertical direction is used more for heat conduction rather than

393 permafrost thawing. The vertical temperature gradient is always negative near the talik
 394 boundary in the permafrost ($\frac{dT}{dn} < 0$) at the center of the lake while the inter-seasonal average
 395 of the horizontal thermal gradient may be negligible ($\frac{dT}{dr} \approx 0$) (McClymont et al., 2013; Devoie
 396 et al., 2021). Assuming the normal heat flux to the phase boundary is uniform throughout the
 397 phase boundary surface ($q_{in,x} = q_{in,z} = q_{in}$), Equation (28) can be simplified as follows:

$$398 \quad \frac{D}{a} = 1 + \frac{k_p}{q_{in}} \frac{dT}{dn} \quad , \text{ or } \quad q_{in} = -\frac{ak_p}{a-D} \frac{dT}{dn} \quad . \quad (29)$$

399 This simple expression may be a useful tool to link the lake depth-width ratio, the lake average
 400 heat flux q_{in} , and the vertical temperature gradient $\frac{dT}{dn}$ at the base of the talik. Since $\frac{dT}{dn} < 0$ in
 401 the permafrost near the talik boundary, the D/a is always less than 1 (flatter than a semi-sphere).
 402 However, the depth-width ratio of the talik depends on the vertical temperature slope near the
 403 talik boundary, which is likely affected by talik age. For instance, Mackay's analytical model
 404 (1962) suggests that the vertical temperature gradient below the lake center begins steeply at the
 405 talik initiation, and then over time it approaches a lower slope at equilibrium. Therefore, the
 406 formula in Equation (29) suggests that a younger talik should be flatter while an older talik
 407 approaches a deeper semi-spheric shape ($D/a \rightarrow 1$).

408 Table 1 shows the estimated incoming heat flux with the key parameters using the proposed
 409 formula (Equation (29)). Creighton et al. (2018) applied the CRYOGRID2 model (Westerman et
 410 al., 2013) to Peatball Lake. The temperature slope at the talik bottom at the lake center was
 411 estimated by the Mackay's analytical model assuming the lake age of 1400 years since the talik
 412 initiation with the same model configuration Creighton et al. (2018) adopted. Creighton et al.
 413 (2018) estimated the interannual mean heat flux q_{in} to be 0.070 (W/m²), which is very close to

414 our estimate. As this simplified formula is consistent with the well-configured modeling result,
415 the horizontal thermal gradient contribution to the vertical aspect ratio of the talik seems to be
416 very small in Peatball Lake.

417 Moreover, this relationship may be useful to incorporate the three-dimensional talik expansion
418 effect in a simple analysis without fully integrated permafrost thermal modeling. For example, if
419 the mean energy flux increases 10 percent from current climate conditions (e.g., shorter lake
420 freeze period), assuming all other properties and horizontal thermal gradient variation are equal,
421 the talik depth-width ratio D/a would shift from 0.171 to 0.234 toward the new equilibrium state.
422 Therefore, this analysis suggests that ~~the a~~ warmer climate may promote permafrost thaw in the
423 vertical direction more than in the horizontal direction. Hence, it is important to quantify the
424 vertical thawing as well as the visible lake horizontal expansion in order to evaluate the impact
425 of the climate change on permafrost thaw beneath thermokarst lakes.

426 **4. Discussion**

427 **4.1 Relationship between hypothetical models**

428 To illustrate the applicability of the thermal model presented here, the available hypothetical
429 models of thermokarst lake growth are compiled in Figure 6. This diagram focuses on the
430 physical processes after the lake initiation stage assuming the bio-ecological effects are
431 negligible.

432 Figure 6 illustrates the evolution of the talik in ice-rich permafrost over time, with driving
433 processes shown in the right panel. In Stage A, the mechanical processes of wave erosion and
434 thaw slumping along lake margins dominate lake expansion in summer, and shallow water favors
435 grounded lake ice in the winter. In time (Stage B), the lake deepens from thaw subsidence

436 beneath the older lake center. Winter ice may freeze to the lake bed, but heat loss is insufficient
437 to freeze the underlying thawed lake bed sediments. A shallow talik develops as thermal
438 processes work in tandem with mechanical processes, the latter now enhanced by more vigorous
439 lake circulation. By Stage C, the talik is well developed beneath the entire lake basin as ground
440 subsidence continues. Eventually (Stage D), the winter ice cover no longer extends to the lake
441 bed, but instead floats atop a residual pool of lake water, while milder vertical temperature
442 gradient beneath the lake deepens the talik as the lake matures. Thermomechanical erosion of
443 lake margins, especially if there are prominent banks in hilly terrain, promotes sedimentation on
444 near-shore shelves, and the underlying talik may begin refreezing. If the lake hasn't drained by
445 this point (Stage E), the talik beneath the lake center extends deeper into the permafrost although
446 subsidence may cease as the excess ice content diminishes with depth. Where many large, old
447 lakes exist, the permafrost may be riddled with deep taliks, and some may eventually penetrate to
448 the permafrost base to create an open-through-going talik.

449 Talik development is affected by a natural processes governed by climatic and local conditions;
450 ~~but can be impacted by direct and indirect human activities.~~ Conditions that favor talik initiation
451 and growth includeing:

- 452 • Deepening lake waters triggered by greater precipitation and/or reduced evaporation,
453 which promotes a floating ice regime
- 454 • Presence of ice-rich sediments (e.g., Yedoma) beneath lakes
- 455 • Warmer lake water induced by regional warming or by longer ice-free summers
- 456 • Thinner winter ice cover due to warmer winter temperatures and/or deeper snow

457 Conversely, talik growth cessation or contraction can occur when these same drivers are
 458 reversed, if the lake partially or completely drains, or when the lake basin is filled with
 459 sediments. The latter scenario is more likely in hilly terrain when the expanding lake erodes
 460 high banks and lake currents redistribute sediments.

461 4.2 Thermal process and preferential expansion

462 4.2.1 Lake geometry and heat balance

463 The analytical expression of the lake geometry may be useful to analyze ~~the~~ horizontally oriented
 464 lakes with direction dependent elongation as well. From Equation (27) and (1), we have,

$$465 \quad a: b = q_{f,x}: q_{f,y} = (q_{in,x} - q_{c,x}): (q_{in,y} - q_{c,y}), \quad (30)$$

466 where a and b are the semi-major and -minor axes of the elongated lake, respectively. When
 467 horizontal heat conduction into the tundra is negligible, ($q_{c,r} = k_p \frac{dT}{dr} \approx 0$), this equation can be
 468 reduced to,

$$469 \quad a: b = q_{in,x}: q_{in,y}. \quad (31)$$

470 Hence, the aspect ratio of elliptic lakes can be explained by heat supply inequality if the lake
 471 geomorphology process is dominated by thermal process. As expressed in Equation (3), there are
 472 two different components in the incoming heat flux to the lake banks: surface energy flux and
 473 heat conduction from the lake water body. Thus, the lake aspect ratio may be written as,

$$474 \quad a: b = \left(q_{suf,x} - k_L \frac{dT}{dx} \right): \left(q_{suf,y} - k_L \frac{dT}{dy} \right) \quad (32)$$

475 **4.2.2 Incoming radiation imbalance effect**

476 One of the incoming surface energy flux inequalities q_{surf} may be caused by shortwave radiation
477 along the lake shoreline. The daily potential solar irradiation on a sloping surface can be
478 computed by the trigonometric function (e.g., Equation B.11 in DeWalle and Rango, 2008). The
479 total daily radiation is a function of latitude and bank slope angle, which depends on the
480 permafrost degradation rate, the maturity of the talik, and ground ice distribution.

481 Figure 7 shows the computed mean daily potential solar irradiation on the sloping lakeshore (I'_q)
482 relative to a flat surface (I_q) during the summer period (June-August) at three different latitudes.
483 The shape of this diagram may correspond to the shape of a thermokarst lake as the enhanced
484 radiation results in more permafrost thaw. The difference in relative incoming radiation will
485 diminish as bank slope angle lessens. In general, the south facing slope along the northern shore
486 tends to receive more radiation than the north facing slope (e.g., Séjourné et al., 2015). This
487 tendency is more pronounced in lower latitude zones due to the higher mid-day sun angle.

488 It is interesting that at 65 and 60 degree latitude the north and south facing banks receive slightly
489 less radiation than east and west facing slopes, while an opposite result occurs at 70 degree
490 latitude (Figure 7). Therefore, the radiation imbalance may partially explain the north-south
491 elongation along the 70 degree latitude line and the west-east elongation of lower latitude (60-65
492 degrees) of lowland thermokarst lakes shown by Grosse et al. (2013, Figure 19). However,
493 because these small differences in incoming radiation imbalance alone are insufficient to result
494 in the distinctive lake elongation in the ACP, they likely introduce rather minor additional
495 complexities in lake spatial shape.

496 **4.3 Wind wave erosion and preferential expansion**

497 Wind wave erosion plays an important role in horizontal expansion of shallow lakes because
498 waves can undercut the vegetated bank (Hopkins, 1949). Wind waves ~~asymptotically~~ makes the
499 water bodies (e.g., lakes and bays) round by local net sediment flux even in low latitude regions
500 (e.g., Ashton et al., 2009). The effect of waves on shoreline morphology has been analyzed in
501 the coastal engineering field: for example, Silvester (1974) investigated the equilibrium shape of
502 bays under different wave conditions using laboratory wave experiments and found that the
503 stable beach in the bay adapted a half-heart or cardioid shape for a fixed wave direction in the
504 absence of sediment supply. Reeve et al. (2018) showed theoretically that the equilibrium
505 coastline shape can be expressed as a diffusion type equation through incorporating the wave
506 diffraction effect, which makes the wave crest line nearly parallel to the shore. However,
507 according to the shallow water wave theory, which is applicable for small fetch distances on
508 lakes in the ACP, water waves do not cause any sediment transport without current, although
509 wave motion is a key factor for the mobilization of the sediment (e.g., Carson and Hussey,
510 1962).

511 Wind-induced water circulation in a shallow, oval lake was perhaps first analyzed by
512 Livingstone (1954) who showed theoretically that the current around the lake ends may be
513 accelerated efficiently by wind-induced return rip currents. However, the lake water circulation
514 pattern assumed in his study (shown in the left side of Figure 8) was less common than the
515 pattern described by Carson and Hussey (1962), who observed reverse circulation patterns near
516 the lake ends, as shown in the right side of Figure 8. For convenience, we refer to two distinctive
517 current patterns: the Livingstone type and the Carson & Hussey (C&H) type. C&H type
518 circulation can indeed explain the commonly observed peat and sediment bars near the leeward

519 lake side shores. Carson and Hussey (1962) noted that sedimentation on the leeward lake side
520 can provide protection from mechanical wave erosion as well as insulation from permafrost
521 thaw, which result in lake elongation. They also observed that preferential bank erosion is
522 typically focused in zones oriented 50 degrees to wave approach. The return flow was found to
523 concentrate around the windward lake side, which accelerates the mechanical erosion and
524 sediment transport at the lake ends. However, the Livingstone type circulation might occur
525 depending on the local wind field as it can explain the sublittoral shelf formation on the
526 windward shore. In either case, the wind-induced current effect on lake elongation can be
527 supported by Livingstone's theory (1954) which should be valid for both circulation types. Thus,
528 the combination of wind wave mobilization and lake water circulation is the most accepted
529 hypothesis for lake elongation during the relatively young shallow lake expansion stage (Carson,
530 1968; Arp et al., 2011, Hinkel et al., 2012).

531 The shallow wave theory states that the sediment mobilization due to wind wave only occurs in
532 shallow water (wave height $>4\%$ of water depth, e.g., Reeve et al., 2018). Therefore, the
533 contribution of the wind wave effect to lake elongation may be reduced as the lake deepens.
534 Figure 9 shows a plot of lake length:width ratios versus the percent of lakes with a bedfast ice
535 regime in seven study regions in Alaska determined with satellite-based synthetic aperture radar
536 imagery (Engram et al., 2018). The study regions represent differences in permafrost
537 characteristics and climate that appear to be reflected in this comparison of length:width ratio
538 and the percent of lakes in a region that freeze to their bed and thus likely do not have a sub-lake
539 talik. For example, lakes in the Teshekpuk Lake and Kuparuk study areas have a shape that is
540 nearly twice as long as it is wide. In both of these regions, more than 80% of the lakes freeze to
541 their bed and likely do not have a talik. This is contrast to lakes located near Umiat and on the

542 Seward Peninsula, that have primarily developed in Yedoma permafrost deposits. Lakes near
543 Umiat and on the Seward Peninsula tend to be more circular ($L:W = 1.3$ to 1.4) and more than
544 90% likely have a talik since they do not freeze to their bed in the winter. The differences
545 observed here relative to elongation of lakes and whether the region primarily has lakes that
546 freeze to their bed or not likely demonstrates a key aspect related to the role of wind-wave
547 erosion. In general, the shallower lakes common in coastal areas, such as Teshekpuk, Barrow,
548 and Kuparuk, are more elongated likely due to wind wave erosion. Whereas lakes in Umiat ([ice-](#)
549 [rich permafrost](#)), Seward Peninsula ([ice-rich permafrost](#)), and Inigok ([ice-poor permafrost](#)) ~~with~~
550 ~~a thicker ice-rich permafrost layer~~ tends to [be](#) rounder because of ~~more rapid~~ talik development
551 and [the presence of deeper lakes \(on the order of 10-20 m in some instances\)](#) ~~more subsequent~~
552 [subsidence](#). This remote-sensing based evidence implies that the wind effect seems to be limited
553 by the lake thermal subsidence due to [sub-lake](#) talik development, ~~underneath~~ while [shallow the](#)
554 [lakes](#) with the bedfast ice may continue elongating by ~~the~~ wind erosion.

555 **4.4 Applicability of the 3D Stefan equation**

556 The limitations of the derived 3D Stefan Equation (Equation 22) are summarized in this section
557 along with Figure 6. Once a seasonal pond is formed on the permafrost, it primarily expands
558 horizontally by wind wave erosion and the thaw slump process ([Livingstone, 1954](#); Carson &
559 Hussey, 1962; [Livingstone, 1954](#); Rex, 1961; Hinkel et al., 2012, Grosse et al., 2013) because
560 the active layer beneath the pond likely freezes every year. On the flat ACP of Alaska, lake thaw
561 [slumps](#) tends to be the result of topography (e.g., slope and aspect of the ground surface) while
562 lake elongation is likely caused by wind wave erosion. As described above, preferential bank
563 thaw at the lake ends can be explained by the insulation effect of the sediments carried by the

564 water current (likely, the C&H type circulation) because the sublittoral shelf may be initiated at
565 this stage.

566 When seasonal thawing penetrates more deeply than the annual freezing depth, a talik may be
567 initiated, typically around the deepest point near the center of the lake (Lachenbruch et al. 1962).
568 Sellmann (1975) described this process, which is one of the mechanisms for shelf formation in a
569 thermokarst lake. For the horizontal expansion stage, A in Figure 6, the proposed quasi-steady
570 state thermal model may not be appropriate because the lakeshore expansion imbalance occurs at
571 least minimally throughout the lake expansion process. However, the 3D Stefan equation may
572 be able to characterize the talik in the initiation stage B in Figure 6.

573 Once the talik is established, the 3D Stefan's thermal model proposed here suggests that the talik
574 may begin to influence lake geometry. Since sediment mobilization due to wind-driven waves
575 occurs in shallow water, lake elongation by waves may diminish as the lake deepens via ground
576 subsidence (Figure 9). Lake water effectively collects energy from the surface during summer
577 and the talik stores the excess heat throughout the winter. Arp et al. (2010, 2011) and Jefferies et
578 al. (1999) discussed the difference in heat conduction between a grounded ice lake and a floating
579 ice lake. Their observations are generally consistent with the proposed theory because a deeper
580 talik under a floating ice lake should have a greater heat capacity. Since lake elongation likely
581 occurs before talik formation, the horizontal lake characterization derived in this study may not
582 be fully applicable to the analysis of thaw lakes on the ACP. In fact, the disagreement of the
583 talik and lake extents in Peatball Lake application illustrates the multiple effects on the lake
584 bathymetry and orientation. Clearly, however, talik expansion and concurrent subsidence
585 stabilizes lake geometry and contributes to lake roundness.

586 The applicability of the proposed 3D Stefan equation ~~must be~~ limited for lakes with high
587 sediment influx and for lakes with through talik. The paired sublittoral shelves on both lake sides
588 are commonly found in the sand dune areas of the southern ACP. The talik shape is likely altered
589 by uneven sediment deposition that affects the temperature gradient normal to the phase
590 boundary as mentioned by several researchers ([Hunter et al., 1981](#); Mackay, 1992; ~~Hunter et al.,~~
591 ~~1981~~; West and Plug, 2008). The shelves created by sediment redistribution due to lake water
592 circulation adds complexity to the ellipsoidal talik shape described in this study. Finally, if the
593 talik penetrates through the permafrost and becomes a throughgoing talik (Hinkel and Arp,
594 2015), the proposed thermal theory herein is no longer applicable for thermokarst lake and talik
595 characterization.

596 **5. Conclusions**

597 The theory presented here addresses the origin of the thermokarst lake ellipticity on the ACP.
598 Elliptic lake geometry results from minimizing overall thawing energy consumption for a given
599 incoming energy load. This is particularly applicable for mature, deep thermokarst lakes with
600 well-developed taliks. Additionally, existing hypothetical models were reviewed to illuminate
601 the thermal effect ([e.g., ellipsoidal talik geometry](#)) on the thermokarst lake morphology.

602 The derived ellipsoid talik model integrates the atmospheric forcing (or incoming energy), the
603 vertical thermal gradient, the thermal diffusivity of the permafrost, and the talik geometry. Heat
604 flux by conduction into the permafrost depends on the heat gradient of the underlying permafrost
605 (Fourier's law). As the vertical temperature slope diminishes with talik maturation, the depth-
606 width ratio of the talik becomes larger creating a deeper talik; thus, much of incoming energy is
607 likely consumed for vertical rather than horizontal expansion. Conversely, during the early

608 stages, thermo-mechanical processes such as wind-driven wave erosion dominates horizontal
609 expansion and elongation of the lake. Consequently, this theory elucidates how talik expansion
610 and concurrent permafrost degradation stabilizes the shape of thermokarst lake to one that is
611 more round rather than elliptical.

612 The semi-ellipsoidal 3D Stefan equation is, to our knowledge, the first geometric model
613 explicitly derived only from the energy conservation equation at the phase boundary. The vector
614 form of the energy conservation equation (Equation 5) in a 3D anisotropic thermal field was
615 integrated at the phase boundary area under the isolated general-shaped lake to quantify the total
616 energy balance. It was shown that the basin total ~~lake fusion~~thaw energy or ~~lake~~-talik expansion
617 rate is equivalent to the weighted phase boundary area. The optimum talik shape function was
618 determined by the variational principle as an extremum of the functional that minimizes the total
619 thawing energy consumption (the stationary action principle). Thus, the resultant semi-ellipsoid
620 equation (Equation 22) can be considered the 3D Stefan equation because it describes the
621 optimum geometry of phase boundary.

622 The derived semi-ellipsoid function was applied to Peatball Lake, ACP of Alaska, where the
623 talik was extensively surveyed using TEM soundings. The pure geometric fitting exercise met
624 the 27 measured TEM data point well with RMSD of 5.94 m, although the talik orientation
625 disagreed with orientation of Peatball Lake and other surrounding lakes. This may be induced by
626 the irregularity due to the rapid and uneven horizontal lake expansion, or possibly by basin
627 coalescence. Comparing the observed talik thickness to the observed lake bathymetry indicated
628 two distinctive permafrost degradation scenarios: significant subsidence by near-surface ice-rich
629 layer thaw and minor contribution of subsidence due to ice-poor permafrost thaw at depth.
630 Consequently, lake water depth is affected by uneven subsidence of thawing permafrost, the

631 interannual water balance; the spatial lake shape irregularity was determined during earlier stage
632 of development. Therefore, careful consideration is required for the analysis of the relationship
633 between lake bathymetry and talik thickness. Nevertheless, this theoretical technique can be
634 used as guidance to partition various effects such as talik development and thaw subsidence,
635 wind wave erosion, lake ice thickness, surficial geology type, and sediment transport by lake
636 water current. Moreover, the analytical expression of the 3D Stefan Equation can be potentially
637 incorporated in the global or regional scale Earth system model to describe missing sub-grid
638 scale processes such as lake dynamics with minimal additional computational resources.

639 **Appendix A: Alternative derivation using isoperimetric inequality**

640 Alternative derivation may provide the thermally optimum talik shape minimizing the phase
641 boundary area A with a fixed talik volume V . Equation (14) establishes talik volume and phase
642 boundary area under the thermokarst lake by a general function of the phase boundary φ . The
643 horizontal coordinate system may be transformed by $(u, v) = \left(\frac{x}{\alpha_x}, \frac{y}{\alpha_y}\right)$. Then, the phase
644 boundary can be expressed as a scaled function,

$$645 \quad \hat{\varphi}(u, v) = \varphi(x, y) = \varphi(\alpha_x u, \alpha_y v), \quad (u, v) \in \hat{B}. \quad (\text{A1})$$

646 According to,

$$647 \quad \begin{cases} \frac{du}{dx} = \frac{1}{\alpha_x}, \\ \frac{dv}{dy} = \frac{1}{\alpha_y}, \\ \frac{\partial}{\partial u} \hat{\varphi}(u, v) = \frac{\partial}{\partial u} \varphi(\alpha_x u, \alpha_y v) = \alpha_x \varphi_x, \\ \frac{\partial}{\partial v} \hat{\varphi}(u, v) = \frac{\partial}{\partial v} \varphi(\alpha_x u, \alpha_y v) = \alpha_y \varphi_y \end{cases} \quad (\text{A2})$$

648 the talik volume and the phase boundary area can be written as,

$$\begin{cases} V[\varphi] = \alpha_x \alpha_y \iint_{\hat{B}} \hat{\varphi} \, dudv \\ A[\varphi] = \alpha_x \alpha_y \iint_{\hat{B}} \sqrt{\hat{\varphi}_u^2 + \hat{\varphi}_v^2 + 1} \, dudv = \alpha_x \alpha_y \int_{\hat{S}} d\hat{S} \end{cases} \quad (A3)$$

650 where \hat{B} denotes the extent of $\hat{\varphi}(u, v)$ on the uv plane, and \hat{S} is the surface on $z = \hat{\varphi}(u, v)$ as,

$$651 \quad \hat{S} = \{ (u, v, z) \in \mathbb{R}^3 \mid (u, v) \in \hat{B}, z = \hat{\varphi}(u, v) \}. \quad (A4)$$

652 The horizontal scaling transform makes it a symmetric closed surface on $z = 0$,

$$653 \quad S^* = \{ (u, v, z) \in \mathbb{R}^3 \mid (u, v) \in \hat{B}, z = \pm \hat{\varphi}(u, v) \}. \quad (A5)$$

654 It is known that volume U enclosed by the ovaloid surface S^* and its surface area satisfy the
655 isoperimetric inequality for an ovaloid surface, which can be written as,

$$656 \quad \left(\int_{S^*} dS^* \right)^3 \geq 36\pi U^2. \quad (A6)$$

657 As the volume and the surface area of the convex closed surface S^* can be expressed as

$$658 \quad U = 2 \left| \iint_{\hat{B}} \hat{\varphi} \, dudv \right| = \frac{2}{\alpha_x \alpha_y} |V[\varphi]|, \text{ and} \quad (A7)$$

$$659 \quad \int_{S^*} dS^* = 2 \int_{\hat{S}} d\hat{S} = \frac{2}{\alpha_x \alpha_y} A[\varphi], \text{ respectively,} \quad (A8)$$

660 we have,

$$661 \quad \left(\frac{2}{\alpha_x \alpha_y} A[\varphi] \right)^3 \geq 36\pi \left(\frac{2}{\alpha_x \alpha_y} V[\varphi] \right)^2, \text{ or}$$

$$662 \quad A[\varphi] \geq \sqrt[3]{18\pi \alpha_x \alpha_y (V[\varphi])^2}. \quad (A9)$$

663 The equality in Equation (A9) holds only if the surface S^* is a sphere, which maximizes the
664 volume. Let the radius of this sphere,

665
$$D = \sqrt[3]{\frac{3}{4\pi}V} = \sqrt[3]{\frac{3|A[\varphi]|}{2\pi\alpha_x\alpha_y}} . \quad (\text{A10})$$

666 From the symmetricity to the plane $z = 0$, we can obtain,

667
$$\hat{\varphi}(u, v) = -D\sqrt{1 - \left(\frac{u}{D}\right)^2 - \left(\frac{v}{D}\right)^2}, \quad (u, v) \in \hat{B}. \quad (\text{A11})$$

668 Inverse scaling coordinate transformation yields the ellipsoid phase boundary function as
669 follows:

670
$$\varphi(x, y) = -D\sqrt{1 - \left(\frac{x}{\alpha_x D}\right)^2 - \left(\frac{y}{\alpha_y D}\right)^2}, \quad (x, y) \in B, \quad (\text{A12})$$

671 where D is the depth of the talik at the center. The ellipsoid, the three-dimensional Stefan
672 Equation for talik, can be obtained by the isoperimetric inequality as well as the functional
673 analysis.

674 **Appendix B: Determination of the coefficients d and λ**

675 We can determine two coefficients in the ellipsoid (Equation 21) by further application of the
676 variational principle. Let

677
$$D = \frac{2}{|\lambda|}. \quad (\text{B1})$$

678 Also, let the intersect d proportional to the vertical radius of the ellipsoid, as follows:

679
$$d = tD \quad (-1 \leq t < 1), \quad (\text{B2})$$

680 where t is a parameter describing the relative elevation of the basin to the original ground
681 surface. Then, Equations (20) and (21) can be rewritten as,

682
$$z = -\varphi = -\sqrt{D^2 - \frac{x^2}{\alpha_x^2} - \frac{y^2}{\alpha_y^2}} + tD \quad , \text{ and} \quad (\text{B3})$$

683
$$\left(\frac{x}{\alpha_x D}\right)^2 + \left(\frac{y}{\alpha_y D}\right)^2 + \left(\frac{z-tD}{D}\right)^2 = 1, \text{ respectively.} \quad (\text{B4})$$

684 Now, the phase boundary area and volume can be evaluated as functions of the parameter t :

685
$$\begin{aligned} V[\varphi] &= \iint_B \varphi \, dx dy = \iint_B \left(-\sqrt{D^2 - \frac{x^2}{\alpha_x^2} - \frac{y^2}{\alpha_y^2}} + tD\right) \, dx dy \\ &= \pi \alpha_x \alpha_y \int_{-(1-t)D}^0 \{D^2 - (tD - z)^2\} dz \\ &= \frac{\pi}{3} \alpha_x \alpha_y D^3 (t^3 - 3t + 2) \end{aligned} \quad (\text{B5})$$

686
$$\begin{aligned} A[\varphi] &= \iint_B \sqrt{\alpha_x^2 \varphi_x^2 + \alpha_y^2 \varphi_y^2 + 1} \, dx dy \\ &= \iint_B \frac{1}{\sqrt{1 - \left(\frac{x}{\alpha_x D}\right)^2 - \left(\frac{y}{\alpha_y D}\right)^2}} \, dx dy \\ &= \pi \alpha_x \alpha_y D^2 \left\{ (1 - t^2) + \int_1^{\frac{1}{z^2}} \left(\frac{1}{z^2} - t^2\right) dz \right\} \\ &= 2\pi \alpha_x \alpha_y D^2 (1 - t) \end{aligned} \quad (\text{B6})$$

687 Eliminating D from these expressions yields,

688
$$A[\varphi]^3 = M \frac{(1-t)^3}{(t^3 - 3t + 2)^2} \quad (\text{B7})$$

689 where M is a positive constant. Therefore, as

690
$$\frac{d}{dt} (A[\varphi]^3) = M \frac{3t}{(1-t)^2 (t+2)^3} > 0 \quad (-1 \leq t < 1), \quad (\text{B8})$$

691 the phase boundary area $A[\varphi]$ is the minimum at $t = 0$. Hence, $d = 0$ that corresponds to a semi-

692 ellipsoid with depth D at the center.

693 **Author contribution**

694 Ohara and Yamatani developed the theory, and all other co-authors, especially Hinkel, Jones,
695 Parsekian, and Kanevskiy, offered crucial advice in interpretation. Jones and Parsekian provided
696 the field observed data for the case study of Peatball Lake. Jones performed the statistical
697 analysis on the oriented lakes based on SAR-satellite remote-sensing data. Ohara prepared the
698 manuscript with contributions from all co-authors.

699 **Acknowledgements**

700 This study was supported by the National Science Foundation (NSF) under awards OPP-
701 1806287, 1806213, and 1806202. The authors thank UIC Science and CH2MHill Polar Field
702 Services (now Battelle Arctic Research Operations) for logistical field support. Datasets and
703 sources code for this research are available in these in-text data citation references. Louise
704 Farquharson and Benjamin Gaglioti provided helpful comments improving the manuscript.

705 **References**

- 706 Arp, C. D., Jones, B. M., Schmutz, J. A., Urban, F. E., & Jorgenson, M. T.: Two mechanisms of
707 aquatic and terrestrial habitat change along an Alaskan Arctic coastline, *Polar Biology*,
708 33(12), 1629-1640, 2010.
- 709 Arp, C. D., Jones, B. M., Urban, F. E., & Grosse, G.: Hydrogeomorphic processes of thermokarst
710 lakes with grounded - ice and floating - ice regimes on the Arctic coastal plain,
711 Alaska, *Hydrological Processes*, 25(15), 2422-2438, 2011.

712 Arp, C. D., Whitman, M. S., Jones, B. M., Kemnitz, R., Grosse, G., & Urban, F. E.: Drainage
713 network structure and hydrologic behavior of three lake-rich watersheds on the Arctic
714 Coastal Plain, Alaska. *Arctic, Antarctic, and Alpine Research*, 44(4), 385-398, 2012.

715 Arp, C. D., Jones, B. M., Liljedahl, A. K., Hinkel, K. M., & Welker, J. A.: Depth, ice thickness,
716 and ice - out timing cause divergent hydrologic responses among Arctic lakes. *Water*
717 *Resources Research*, 51(12), 9379-9401, 2015.

718 Arp, C. D., Jones, B. M., Grosse, G., Bondurant, A. C., Romanovsky, V. E., Hinkel, K. M., &
719 Parsekian, A. D.: Threshold sensitivity of shallow Arctic lakes and sublake permafrost to
720 changing winter climate, *Geophysical Research Letters*, 43(12), 6358-6365, 2016.

721 Ashton, A.D., Murray, A.B., Littlewood, R., Lewis, D.A. and Hong, P.: Fetch-limited self-
722 organization of elongate water bodies, *Geology*, 37(2), pp.187-190, 2009.

723 Black, R. F., & Barksdale, W. L.: Oriented lakes of northern Alaska, *The Journal of Geology*,
724 57(2), 105-118, 1949.

725 Brewer, M. C.: The thermal regime of an arctic lake, *Eos, Transactions American Geophysical*
726 *Union*, 39(2), 278-284, 1958.

727 Burn, C. R., & Smith, M. W.: Development of thermokarst lakes during the Holocene at sites
728 near Mayo, Yukon Territory, *Permafrost and Periglacial Processes*, 1(2), 161-175, 1990.

729 Burn, C.R.: Tundra lakes and permafrost, Richards Island, western Arctic coast, Canada,
730 *Canadian Journal of Earth Sciences*, 39(8), pp.1281-1298, 2002.

731 Carslaw, H. S., & Jaeger, J. C.: *Conduction of heat in solids*. Oxford: Clarendon Press, 1959.

- 732 Carson, C. E.: Radiocarbon dating of lacustrine strands in Arctic Alaska. *Arctic*, 12-26, 1968.
- 733 Carson, C. E., & Hussey, K. M.: The oriented lakes of Arctic Alaska, *The Journal of Geology*,
- 734 70(4), 417-439, 1962.
- 735 Carter, L. D.: A Pleistocene sand sea on the Alaskan Arctic coastal plain, *Science*, 211(4480),
- 736 381-383, 1981.
- 737 Cassel, K. W.: Variational methods with applications in science and engineering, Cambridge
- 738 University Press, 2013.
- 739 Courant, R., & Hilbert, D.: Methods of mathematical physics, *Bulletin of the American*
- 740 *Mathematical Society*, 60, 578-579, 1954.
- 741 Creighton, A. L., Parsekian, A. D., Angelopoulos, M., Jones, B. M., Bondurant, A., Engram,
- 742 M., ... & Arp, C. D.: Transient electromagnetic surveys for the determination of talik
- 743 depth and geometry beneath thermokarst lakes, *Journal of Geophysical Research: Solid*
- 744 *Earth*, 123(11), 9310-9323, 2018.
- 745 Czudek, T. and Demek, J.: Thermokarst in Siberia and its influence on the development of
- 746 lowland relief, *Quaternary Research*, 1(1), pp.103-120, 1970.
- 747 Devoie, É.G., Craig, J.R., Dominico, M., Carpino, O., Connon, R.F., Rudy, A.C. and Quinton,
- 748 W.L.: Mechanisms of Discontinuous Permafrost Thaw in Peatlands, *Journal of*
- 749 *Geophysical Research: Earth Surface*, 126(11), p.e2021JF006204, 2021.
- 750 DeWalle, D. R., & Rango, A.: Principles of snow hydrology, Cambridge University Press, 2008.

751 Doolittle, J. A., Hardisky, M. A., & Gross, M. F.: A ground-penetrating radar study of active
752 layer thicknesses in areas of moist sedge and wet sedge tundra near Bethel, Alaska, USA.
753 Arctic and Alpine Research, 22(2), 175-182, 1990.

754 Engram, M., Arp, C. D., Jones, B. M., Ajadi, O. A., & Meyer, F. J.: Analyzing floating and
755 bedfast lake ice regimes across Arctic Alaska using 25 years of space-borne SAR
756 imagery. Remote sensing of environment, 209, 660-676, 2018.

757 [French, H. M.: The Periglacial Environment, Longman, New York, 1996.](#)

758 Farquharson, L., Anthony, K.W., Bigelow, N., Edwards, M. and Grosse, G.: Facies analysis of
759 yedoma thermokarst lakes on the northern Seward Peninsula, Alaska. Sedimentary
760 Geology, 340, pp.25-37, 2016.

761 [French, H.M. 2018. The Periglacial Environment. 4th ed. John Wiley and Sons Ltd., Chichester,](#)
762 [UK, 515 pp.](#)

763 Gelfand, I. M., & Fomin, S. V.: Calculus of variations. Revised English edition translated and
764 edited by Richard A. Silverman. *Prentice Hall, Englewood Cliffs, NJ*, 7, 10-11, 1963.

765 Grosse, G., Jones, B. M., & Arp, C. D.: Thermokarst lakes, drainage, and drained basins. In:
766 Shroder, J. (Editor in Chief), Giardino, R., Harbor, J. (Eds.), *Treatise on Geomorphology*.
767 Academic Press, San Diego, CA, vol. 8, *Glacial and Periglacial Geomorphology*, pp.
768 325–353, 2013.

769 Heslop, J.K., Walter Anthony, K.M., Sepulveda-Jauregui, A., Martinez-Cruz, K., Bondurant, A.,
770 Grosse, G. and Jones, M.C.: Thermokarst lake methanogenesis along a complete talik
771 profile, *Biogeosciences*, 12(14), pp.4317-4331, 2015.

772 Hinkel, K. M., Frohn, R. C., Nelson, F. E., Eisner, W. R., & Beck, R. A.: Morphometric and
773 spatial analysis of thaw lakes and drained thaw lake basins in the western Arctic Coastal
774 Plain, Alaska, *Permafrost and Periglacial Processes*, 16(4), 327-341, 2005.

775 Hinkel, K. M., Sheng, Y., Lenters, J. D., Lyons, E. A., Beck, R. A., Eisner, W. R., & Wang, J.:
776 Thermokarst lakes on the Arctic coastal plain of Alaska: geomorphic controls on
777 bathymetry, *Permafrost and Periglacial Processes*, 23(3), 218-230, 2012.

778 Hinkel, K. M., & Arp, C.: Estimating talik depth beneath lakes in Arctic Alaska, In Proceedings,
779 7th Canadian Permafrost Conference and 68th Canadian Geotechnical Conference, pp.
780 20-23, 2015.

781 Hopkins, D. M.: Thaw lakes and thaw sinks in the Imuruk Lake area, Seward Peninsula, Alaska,
782 *The Journal of Geology*, 57(2), 119-131, 1949.

783 Hopkins, D. M., Karlstrom, T., Black, R., Williams, J., Pewe, T., Fernold, A., & Muller, E.:
784 Permafrost and ground water in Alaska, a shorter contribution to the general geology. US
785 Geol. Surv. Prof. Pap, 264, 1955.

786 Hunter, J. A., MacAulay, H. A., Gagné, R. M., Burns, R. A., Harrison, T. E., & Hawkins, J. P.:
787 Drained lake experiment for investigation of growth of permafrost at Illisarvik,
788 Northwest Territories—initial geophysical results, *Current research, part C. Geological*
789 *Survey of Canada, Paper*, 67-76, 1981.

790 Jeffries, M.O., Morris, K. and Liston, G.E.: A method to determine lake depth and water
791 availability on the North Slope of Alaska with spaceborne imaging radar and numerical
792 ice growth modelling. *Arctic*, pp.367-374, 1996.

793 Jeffries, M. O., Morris, K., Maksym, T., Kozlenko, N., & Tin, T.: Autumn sea ice thickness,
794 ridging and heat flux variability in and adjacent to Terra Nova Bay, Ross Sea, Antarctica,
795 *Journal of Geophysical Research: Oceans*, 106(C3), 4437-4448, 2001.

796 Johnston, G. H., & Brown, R. J. E.: Occurrence of permafrost at an Arctic lake, *Nature*,
797 211(5052), 952-953, 1966.

798 Jones, B. M., Grosse, G. D. A. C., Arp, C. D., Jones, M. C., Anthony, K. W., & Romanovsky, V.
799 E.: Modern thermokarst lake dynamics in the continuous permafrost zone, northern
800 Seward Peninsula, Alaska, *Journal of Geophysical Research: Biogeosciences*, 116(G2),
801 2011.

802 [Jones, B.M., Grosse, G., Farquharson, L.M, Roy-Léveillé, P., Veremeeva A., Kanevskiy, M.Z.,](#)
803 [Gaglioti, B.V., Breen, A.L., Parsekian, A.D., Ulrich, M., and Hinkel, K.M.:~~2022~~. Lake](#)
804 [and drained lake basin systems in lowland permafrost regions. *Nature Reviews Earth and*](#)
805 [Environment 3: 85-98. <https://doi.org/10.1038/s43017-021-00238-9>, ~~2022~~.](#)

806 [Jorgenson, M.T.:~~2013~~. Thermokarst terrains. In: Shroder, J. \(Editor in Chief\), Giardino, R.,](#)
807 [Harbor, J. \(Eds.\), *Treatise on Geomorphology*. Academic Press, San Diego, CA, vol. 8,](#)
808 [Glacial and Periglacial Geomorphology, pp. 313–324, ~~2013~~.](#)

809 Jorgenson, M. T., & Shur, Y.: Evolution of lakes and basins in northern Alaska and discussion of
810 the thaw lake cycle, *Journal of Geophysical Research: Earth Surface*, 112(F2), 2007.

811 [Jorgenson, T., Yoshikawa, K., Kanevskiy, M., Shur, Y., Romanovsky, V., Marchenko, S.,](#)
812 [Grosse, G., Brown, J., and Jones, B.:~~2008~~. Permafrost characteristics of Alaska. In:](#)
813 [Proceedings of the 9th International Conference on Permafrost, Extended Abstracts. June](#)

814 [29–July 3, 2008, Fairbanks, AK. Kane, D.L., and Hinkel, K.M. \(Eds.\), Institute of](#)
815 [Northern Engineering, University of Alaska Fairbanks: 121–122, 2008.](#)

816 Kanevskiy, M., Shur, Y., Fortier, D., Jorgenson, M. T., & Stephani, E.: Cryostratigraphy of late
817 Pleistocene syngenetic permafrost (yedoma) in northern Alaska, Itkillik River exposure.
818 *Quaternary research*, 75(3), 584-596, 2011.

819 Kanevskiy, M., Shur, Y., Jorgenson, M. T., Ping, C. L., Michaelson, G. J., Fortier, D., ... &
820 Tums koy, V.: Ground ice in the upper permafrost of the Beaufort Sea coast of Alaska,
821 *Cold Regions Science and Technology*, 85, 56-70, 2013.

822 ~~Kanevskiy, M., Shur, Y., Strauss, J., Jorgenson, T., Fortier, D., Stephani, E., & Vasiliev, A.:~~
823 ~~Patterns and rates of riverbank erosion involving ice rich permafrost (yedoma) in~~
824 ~~northern Alaska, *Geomorphology*, 253, 370-384, 2016.~~

825 ~~Kanevskiy, M., and K. Bjella.: A Permafrost Primer for Highway and Airport Engineers, Final~~
826 ~~report, Alaska Department of Transportation and Public Facilities, AKDOT&PF Report~~
827 ~~No. 000S927a, 2020.~~

828 Kessler, M. A., Plug, L. J., & Anthony, K. W.: Simulating the decadal - to millennial - scale
829 dynamics of morphology and sequestered carbon mobilization of two thermokarst lakes
830 in NW Alaska, *Journal of Geophysical Research: Biogeosciences*, 117(G2), 2012.

831 Kurylyk, B. L., & Hayashi, M.: Improved Stefan equation correction factors to accommodate
832 sensible heat storage during soil freezing or thawing. *Permafrost and Periglacial*
833 *Processes*, 27(2), 189-203, 2016.

834 Lachenbruch, A.H., Brewer, M.C., Greene, G.W., Marshall, B.V.: Temperatures in permafrost,
835 In Temperature—Its Measurement and Control in Science and Industry, 3, Herzfeld CM
836 (ed). Reinhold Publishing: New York; 791–803, 1962.

837 Lenz J, Jones BM, Wetterich S, Tjallingii R, Fritz M, Arp CD, Rudaya N, Grosse G. Impacts of
838 shore expansion and catchment characteristics on lacustrine thermokarst records in
839 permafrost lowlands, Alaska Arctic Coastal Plain. *arktos*. 2016 Dec;2(1):1-5., 2016.

840 Ling, F., & Zhang, T.: Impact of the timing and duration of seasonal snow cover on the active
841 layer and permafrost in the Alaskan Arctic, *Permafrost and Periglacial Processes*, 14(2),
842 141-150, 2003a.

843 Ling, F., and T. Zhang: Numerical simulation of permafrost thermal regime and talik
844 development under shallow thaw lakes on the Alaskan Arctic Coastal Plain, *J. Geophys.*
845 *Res.*, 108(D16), 4511, doi:10.1029/2002JD003014, 2003b.

846 Livingstone, D.A.: On the orientation of lake basins, *American Journal of Science*, 252: 547–
847 554, 1954.

848 Lunardini, V.J.: *Heat Transfer in Cold Climates*, Van Nostrand Reinhold Co.: New York, NY;
849 731, 1981.

850 Mackay J.R.: The Mackenzie Delta area, N.W.T. Geographical Branch Memoir 8, Department of
851 Mines and Technical Surveys, Ottawa, 1963.

852 Mackay, J.R.: Lake stability in an ice-rich permafrost environment: examples from the western
853 Arctic coast. In: Robarts, R.D., Bothwell, M.L. (Eds.), *Aquatic Ecosystems in Semi-Arid*

- 854 Regions: Implications for Resource Management. NHRI Symposium Series 7.
855 Environment Canada, Saskatoon, Saskatchewan, pp. 1–26, 1992.
- 856 McClymont, A.F., Hayashi, M., Bentley, L.R. and Christensen, B.S.: Geophysical imaging and
857 thermal modeling of subsurface morphology and thaw evolution of discontinuous
858 permafrost, *Journal of Geophysical Research: Earth Surface*, 118(3), pp.1826-1837,
859 2013.
- 860 Ohara N., and Yamatani K.: Theoretical Stable Hydraulic Section based on the Principle of Least
861 Action. *Scientific Reports*, 9, Article number: 7957, 2019.
- 862 O’Neill, H. B., Roy - Leveillee, P., Lebedeva, L., & Ling, F.: Recent advances (2010-2019) in
863 the study of taliks, *Permafrost and Periglacial Processes*, 31(3), 346-357, 2020.
- 864 Parsekian, A. D., Creighton, A. L., Jones, B. M., & Arp, C. D.: Surface nuclear magnetic
865 resonance observations of permafrost thaw below floating, bedfast, and transitional ice
866 lakes, *Geophysics*, 84(3), EN33-EN45, 2019.
- 867 Painter, S. L., Coon, E. T., Atchley, A. L., Berndt, M., Garimella, R., Moulton, J. D., ... &
868 Wilson, C. J.: Integrated surface/subsurface permafrost thermal hydrology: Model
869 formulation and proof - of - concept simulations, *Water Resources Research*, 52(8),
870 6062-6077, 2016.
- 871 Patel, P. D.: Interface conditions in heat-conduction problems with change of phase, *AIAA*
872 *Journal*, 6(12), 2454-2454, 1968.
- 873 Pilon, J. A., Annan, A. P., & Davis, J. L.: Monitoring permafrost ground conditions with ground
874 probing radar (GPR), In Workshop on Permafrost Geophysics, Golden, Colorado. US

875 Army Corps of Engineers, Cold Regions Research and Engineering Laboratory, Hanover,
876 New Hampshire, CRREL Special Report (pp. 85-5), 1985.

877 Plug, L. J., & West, J. J.: Thaw lake expansion in a two - dimensional coupled model of heat
878 transfer, thaw subsidence, and mass movement, *Journal of Geophysical Research: Earth*
879 *Surface*, 114(F1), 2009.

880 Rampton, V. N.: Quaternary geology of the Yukon coastal plain, 1982.

881 Rangel R.C., A. D. Parsekian, L. M. Farquharson, B. M. Jones, N. Ohara, A. L. Creighton, B. V.
882 Gaglioti, M. Kanevskiy, A. L. Breen, H. Bergstedt, V. E. Romanovsky, and K. M.
883 Hinkel.: Geophysical Observations of Taliks Below Drained Lake Basins on the Arctic
884 Coastal Plain of Alaska. *Journal of Geophysical Research: Solid Earth* 126,
885 e2020JB020889. <https://doi.org/10.1029/2020JB020889>, 2020.

886 Reeve, D., Chadwick, A., & Fleming, C.: Coastal engineering: processes, theory and design
887 practice, CRC Press, 2018.

888 Rex, R. W.: Hydrodynamic analysis of circulation and orientation of lakes in Northern Alaska. In
889 *Geology of the Arctic*, Rauch GO (ed). University of Toronto Press: Toronto; 1021–
890 1043, 1961.

891 Rowland, J. C., B. J. Travis, and C. J. Wilson: The role of advective heat transport in talik
892 development beneath lakes and ponds in discontinuous permafrost, *Geophys. Res. Lett.*,
893 38, L17504, doi:10.1029/2011GL048497, 2011.

894 Roy-Leveillee, P., & Burn, C. R.: Near - shore talik development beneath shallow water in
895 expanding thermokarst lakes, Old Crow Flats, Yukon, Journal of Geophysical Research:
896 Earth Surface, 122(5), 1070-1089, 2017.

897 ~~Rowland, J. C., B. J. Travis, and C. J. Wilson: The role of advective heat transport in talik~~
898 ~~development beneath lakes and ponds in discontinuous permafrost, Geophys. Res. Lett.,~~
899 ~~38, L17504, doi:10.1029/2011GL048497, 2011.~~

900 Schirrmeister, L., Froese, D., Tums koy, V., Grosse, G., and Wetterich, S.: 2013. Yedoma: Late
901 Pleistocene ice-rich syngenetic permafrost of Beringia. Encyclopedia of Quaternary
902 Science, 2nd ed., pp. 542–552, 2013.

903 Schuur, E. A., McGuire, A. D., Schädel, C., Grosse, G., Harden, J. W., Hayes, D. J., ... & Natali,
904 S. M.: Climate change and the permafrost carbon feedback. Nature, 520(7546), 171-179,
905 2015.

906 Schwamborn, G., Andreev, A., Rachold, V., Hubberten, H. W., Grigoriev, M. N., Tums koy,
907 V., ... & Dorozkhina, M. V.: Evolution of Lake Nikolay, Arga Island, Western Lena
908 River delta, during late Pleistocene and Holocene time, Polarforschung, 70, 69-82, 2000.

909 Séjourné, A., Costard, F., Fedorov, A., Gargani, J., Skorve, J., Massé, M., & Mège, D.:
910 Evolution of the banks of thermokarst lakes in Central Yakutia (Central Siberia) due to
911 retrogressive thaw slump activity controlled by insolation. Geomorphology, 241, 31-40,
912 2015.

913 Sellmann, P. V.: *The classification and geomorphic implications of thaw lakes on the Arctic*
914 *Coastal Plain, Alaska* (Vol. 344), US Department of Defense, Department of the Army,

915 Corps of Engineers, Cold Regions Research and Engineering Laboratory, Report. 21 pp,
916 1975.

917 ~~Séjourné, A., Costard, F., Fedorov, A., Gargani, J., Skorve, J., Massé, M., & Mège, D.:~~
918 ~~Evolution of the banks of thermokarst lakes in Central Yakutia (Central Siberia) due to~~
919 ~~retrogressive thaw slump activity controlled by insolation. *Geomorphology*, 241, 31–40,~~
920 ~~2015.~~

921 [Shur, Y., and Osterkamp, T.: 2007. Thermokarst. Report INE 06.11. University of Alaska](#)
922 [Fairbanks, Institute of Northern Engineering, Fairbanks, AK \(50 pp.\), 2007.](#)

923 Silvester, R., & Hsu, J. R.: Coastal Stabilization, Advanced Series on Ocean Engineering, Vol.
924 14, 1997.

925 [Singer-Loginova, I., & Singer, H. M.: The phase field technique for modeling multiphase](#)
926 [materials. *Reports on progress in physics*, 71\(10\), 106501, 2008.](#)

927 Stefan J.: Über die Theorie der Eisbildung, insbesondere über die Eisbildung im Polarmee.
928 *Annals of Physics and Chemistry* 42: 269–286, 1891.

929 ~~Schwamborn, G., Andreev, A., Rachold, V., Hubberten, H. W., Grigoriev, M. N., Tumskey,~~
930 ~~V., ... & Dorozkhina, M. V.: Evolution of Lake Nikolay, Arga Island, Western Lena~~
931 ~~River delta, during late pleistocene and holocene time, *Polarforschung*, 70, 69–82, 2000.~~

932 Sullivan, T. D., Parsekian, A. D., Sharp, J., Hanke, P. J., Thalasso, F., Shapley, M., ... & Walter
933 Anthony, K.: Influence of permafrost thaw on an extreme geologic methane seep.
934 *Permafrost and Periglacial Processes*, 2021.

935 Tomirdiaro, S. V.: Evolution of lowland landscapes in northeastern Asia during late Quaternary
936 time, In Paleocology of Beringia (pp. 29-37). Academic Press, 1982.

937 van Everdingen, R.O. (Ed.): Multi-Language Glossary of Permafrost and Related Ground-ice
938 Terms, International Permafrost Association, The Arctic Institute of North America,
939 University of Calgary, Calgary, 268 pp, 1998.

940 West, J. J., and L. J. Plug: Time-dependent morphology of thaw lakes and taliks in deep and
941 shallow ground ice, J. Geophys. Res., 113, F01009, doi:10.1029/2006JF000696, 2008.

942 Westermann, S., Schuler, T. V., Gislås, K., & Etzelmüller, B.: Transient thermal modeling of
943 permafrost conditions in Southern Norway, The Cryosphere, 7(2), 719-739, 2013.

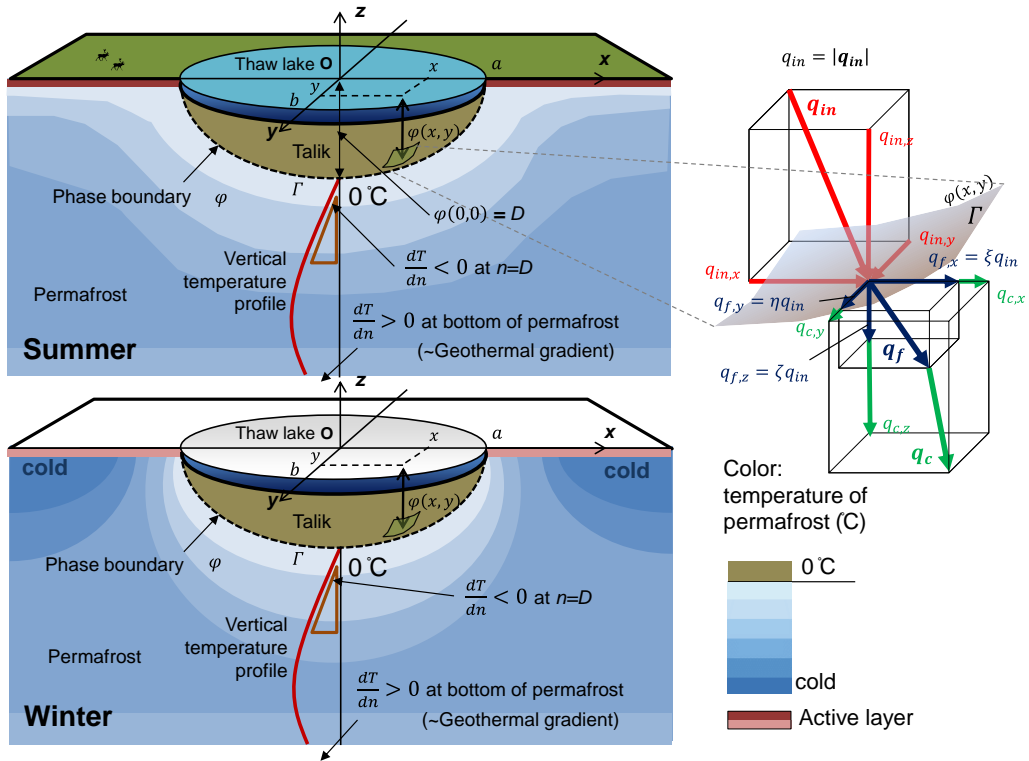
944 ~~van Everdingen, R.O. (Ed.): Multi-Language Glossary of Permafrost and Related Ground-ice~~
945 ~~Terms, International Permafrost Association, The Arctic Institute of North America,~~
946 ~~University of Calgary, Calgary, 268 pp, 1998.~~

947 Table 1: Computed incoming heat flux with the estimated parameters

Parameter	Estimates	Unit	Note
Porosity	0.18		Sandstone >15 m deep; Creighton et al., 2018
Thermal conductivity of permafrost	2.20	W/(m·K)	From porosity and typical thermal properties of ice and mineral in this region
Talik depth, D	88.0	m	Fitted ellipsoid
Talik width (radius), a	514.8	m	Fitted ellipsoid
Aspect ratio, D/a	0.1709		Fitted ellipsoid
Geothermal gradient	0.0250	K/m	Kessler et al., 2012
dT/dz at the talik bottom	-0.0259	K/m	From Mackay model (1962)
Basin average heat flux, q_{in}	0.0689	W/m ²	Computed from Equation (29)

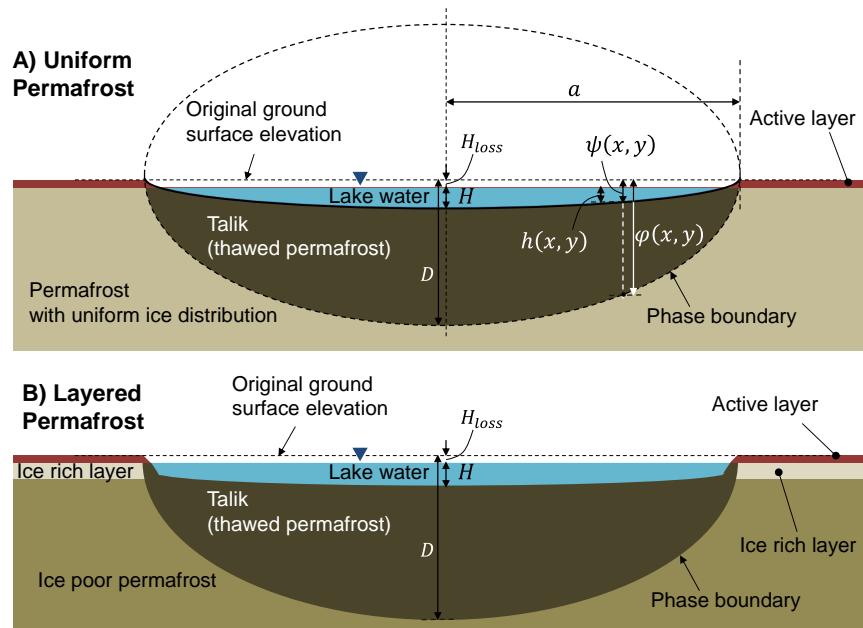
948

949



950
 951
 952
 953
 954
 955
 956

Figure 1: Definitions of variables associating with the overall shape of phase boundary φ during warm (Upper left panel) and cold seasons (Lower left panel) and incoming and outgoing heat transfers on $\varphi(x, y)$ (Right panel). Incoming heat (red colored vector) is perpendicular to the phase boundary $\varphi(x, y)$ while thaw direction (blue colored vector) is modified by the anisotropic heat conduction (green colored vector) in the permafrost.



957

958

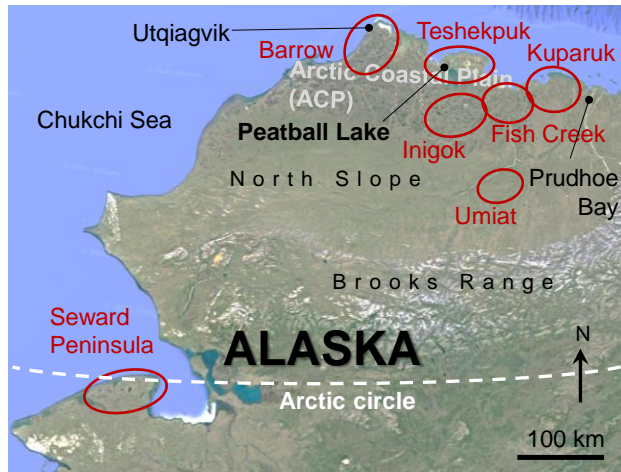
959

960

961

962

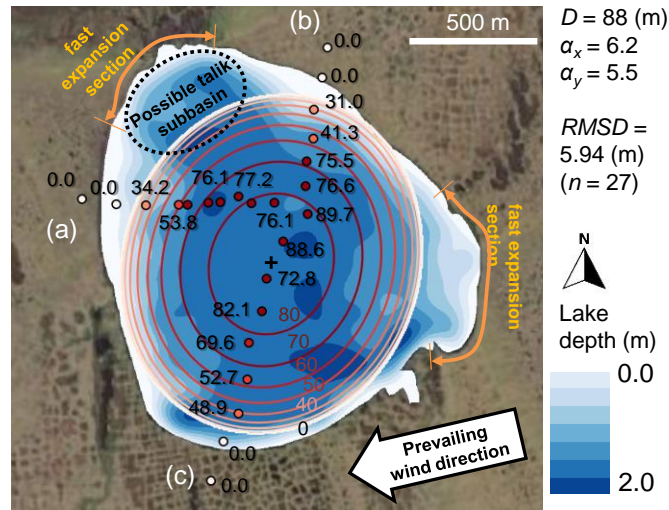
Figure 2: Lake bathymetry models for a thermokarst lake and the talik underneath based on the quasi-steady state. (A) The lake bathymetry is proportional to the talik geometry with uniform ice distribution. (B) However, the lake bathymetry tends to have a flat bottom due to the widespread ice-rich layer near the surface.



963

964 Figure 3: Map of the study area: Peatball Lake and subregions for lake characterization (red).

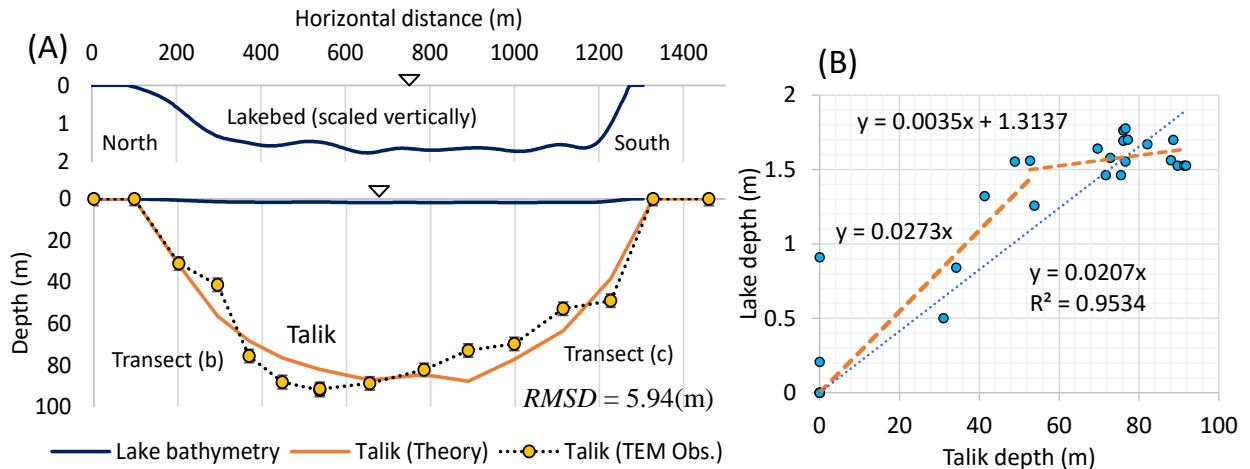
965



966

967 Figure 4: The theoretically extrapolated talik thickness map (contour lines) based on 27 TEM soundings
 968 (dots) in Peatball Lake, ACP of Alaska. The red contour lines and the observation points are consistent.
 969 The corresponding observed lake bathymetry (adopted from Lenz et al., 2016) is also included in blue
 970 gradation. The TEM sounding transects start on the lakeshore and end near the center of the lake.

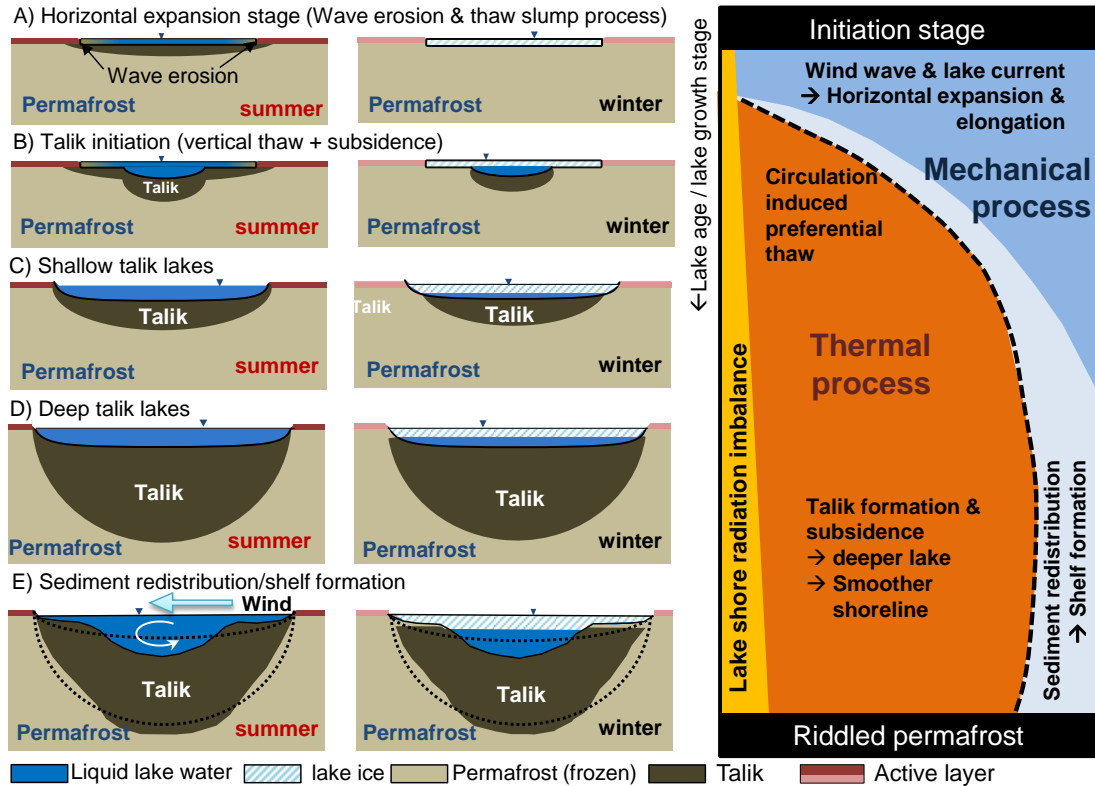
971



972

973 Figure 5: Cross sectional comparisons of the lakebed and the talik profiles along two TEM transects (b)
 974 through (c) (Lenz et al., 2016) in Peatball Lake. Panel (B) displays the cross plot of the observed talik
 975 and lake depths at all 27 TEM data points.

976



977

978

979

980

981

982

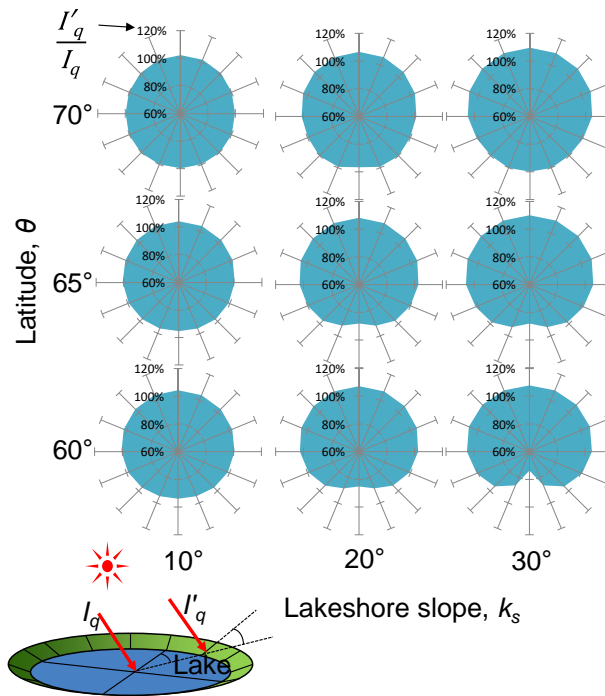
983

984

985

986

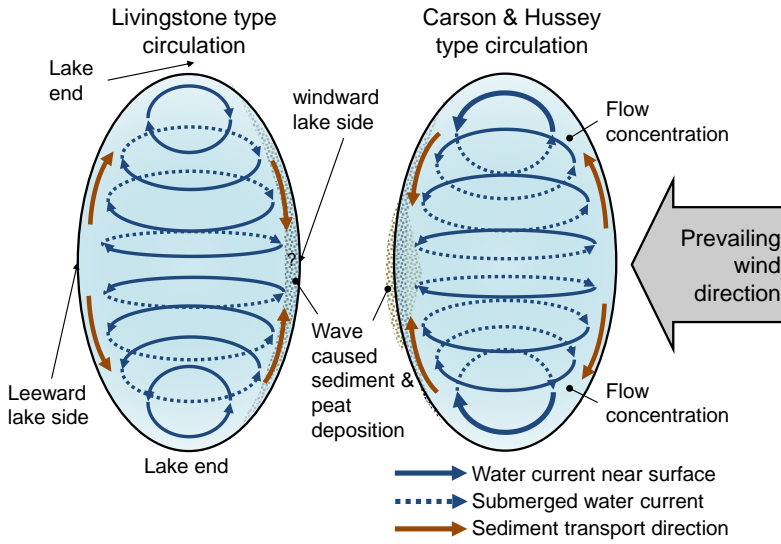
Figure 6: Combined hypothetical models of thermokarst lake evolution and diagram of major influencing factors through time. The left column represents summer conditions, the center column represents winter conditions, and the right column indicates the corresponding importance of mechanical vs. thermal processes through time as the lake ages (top is younger, bottom is older). Row (A) indicates the early processes under bedfast ice conditions before talik initiation. Row (B) shows the onset of vertical thaw and subsidence as talik begins to develop. Row (C) shows early, shallow talik growth conditions. Row (D) indicates later stage processes on deepened talik due to vertical thaw. Row (E) is the mature stage of development when complex bathymetry has set in as a result of sediment transport.



987

988 Figure 7: Computed mean daily potential solar radiation on sloping lakeshore relative to the flat surface
 989 during summer period (June-August) with respect to latitude. I_q is the potential solar radiation on a flat
 990 surface, and I'_q is radiation on sloping lakeshore.

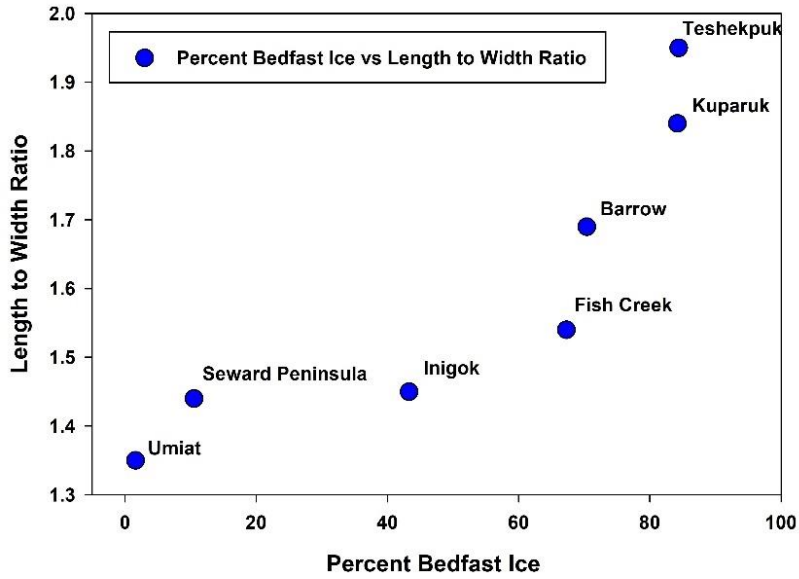
991



992

993 Figure 8: Two distinctive lake water circulation patterns created by unidirectional wind. Livingstone type
 994 circulation (Left) and Carson & Hussey type circulation (Right) causes opposite flow directions around
 995 lake ends. This also results in difference in sediment and peat deposition patterns.

996



997

998

Figure 9: Comparison of Length to Width ratio versus the percent of a particular region exhibiting a

999

bedfast lake ice regime for seven study areas in Arctic Alaska. This analysis is based on SAR-satellite

1000

remote-sensing data presented in Engram et al. (2018). Lakes that are more elliptical in shape tend to

1001

occur where the majority of the lakes in the area freeze to their bed and thus likely do not have a talik.

1002

Lakes that are more circular in shape tend to occur where the majority of lakes in an area do not freeze to

1003

their bed and thus likely have a sub-lake talik.

1004